Meteoritics & Planetary Science 39, Nr 9, 1419–1447 (2004)
Abstract available online at http://meteoritics.org

Lunar highland meteorite Dhofar 026 and Apollo sample 15418: Two strongly shocked, partially melted, granulitic breccias

Barbara A. COHEN,[1, 2†] Odette B. JAMES,[3*] Lawrence A. TAYLOR,[1]
Mikhail A. NAZAROV,[4] and Larisa D. BARSUKOVA[4]

[1]Planetary Geosciences Institute, University of Tennessee, Knoxville, Tennessee 37996, USA
[2]Hawaii Institute of Geophysics and Planetology, University of Hawaii, Honolulu, Hawaii 96822, USA
[3]Emeritus, U. S. Geological Survey, Reston, Virginia 20192, USA
[4]Vernadsky Institute of Geochemistry and Analytical Chemistry, Moscow 199991, Russia
[†]Present Address: Institute of Meteoritics, Department of Earth and Planetary Sciences, University of New Mexico, Albuquerque, New Mexico 87131, USA
[*]Corresponding author. E-mail: ojames@usgs.gov

(Received 15 October 2003; revision accepted 2 July 2004)

Abstract–Studies of lunar meteorite Dhofar 026, and comparison to Apollo sample 15418, indicate that Dhofar 026 is a strongly shocked granulitic breccia (or a fragmental breccia consisting almost entirely of granulitic breccia clasts) that experienced considerable post-shock heating, probably as a result of diffusion of heat into the rock from an external, hotter source. The shock converted plagioclase to maskelynite, indicating that the shock pressure was between 30 and 45 GPa. The post-shock heating raised the rock's temperature to about 1200 °C; as a result, the maskelynite devitrified, and extensive partial melting took place. The melting was concentrated in pyroxene-rich areas; all pyroxene melted. As the rock cooled, the partial melts crystallized with fine-grained, subophitic-poikilitic textures. Sample 15418 is a strongly shocked granulitic breccia that had a similar history, but evidence for this history is better preserved than in Dhofar 026. The fact that Dhofar 026 was previously interpreted as an impact melt breccia underscores the importance of detailed petrographic study in interpretation of lunar rocks that have complex textures. The name "impact melt" has, in past studies, been applied only to rocks in which the melt fraction formed by shock-induced total fusion. Recently, however, this name has also been applied to rocks containing melt formed by heating of the rocks by conductive heat transfer, assuming that impact is the ultimate source of the heat. We urge that the name "impact melt" be restricted to rocks in which the bulk of the melt formed by shock-induced fusion to avoid confusion engendered by applying the same name to rocks melted by different processes.

INTRODUCTION

Dhofar 026 is a 148 g, brownish-gray, stony meteorite discovered in Oman in March 2000. The rock is a lunar breccia of gabbroic-anorthosite bulk composition with no fusion crust and little terrestrial weathering. To characterize this meteorite, we have determined its bulk composition, texture, and mineral compositions. Our data and oxygen isotope data (Taylor et al. 2001) indicate that the meteorite is a lunar rock.

We initially interpreted Dhofar 026 as an impact melt (Cohen et al. 2001; Taylor et al. 2001). Detailed study of the texture and mineralogy of this rock and comparison to Apollo sample 15418, however, indicate that both rocks are shocked breccias that were partially melted by post-shock heating. Because these rocks provide excellent examples of textural complexity induced by shock and subsequent heating, our work elucidates parameters that help interpret the textures of rocks with such histories and indicates characteristics useful in distinguishing shock-generated impact melts from rocks that were melted by conductive transfer of heat from nearby, higher temperature material. The results have application to the study of all lunar and meteoritic samples with similar complex histories. A summary of our studies was presented by James et al. (2003).

ANALYTICAL TECHNIQUES

A polished section of Dhofar 026 (area: ~78 mm^2), obtained from the Vernadsky Institute, was examined with a

petrographic microscope. Mineral modes were estimated from backscattered electron (BSE) images taken with a scanning electron microscope (SEM), either by classifying pixels and using the histogram function in Adobe Photoshop or by point counting using a transparent grid laid over the images (630–850 points per count). Mineral compositions (Tables 1–4) were determined at the University of Tennessee and at the University of Hawaii with Cameca SX50 electron microprobes (EMP) using synthetic and mineral standards, a 15 kV excitation potential, and a 20 nA beam current; ZAF corrections (Cameca PAP) were applied. Defocused-beam EMP analyses (~30 μm beam size) were used to determine bulk compositions of several types of materials in the rock. These analyses are presented (Table 5) as uncorrected averages and averages corrected for density differences among the phases within the analyzed areas (Warren 1997). To perform the corrections, we calculated ß factors (Warren 1997) for each element using a mode of the analyzed area determined by point counting, average phase analyses from Tables 1–3, phase densities from the literature or a normative calculation, and density of the bulk material from a normative calculation. The corrected composition, derived by multiplying each element by its ß factor, was used to calculate a new bulk density, which was then used for a second iteration. It should be noted that uncertainties in the mode and the average phase compositions lead to large uncertainties in the correction. Further details are given in Table 5. Normative mineralogies and bulk densities were calculated using CIPW norm software by Kurt Hollocher (Union College, Schenectady, New York).

At the Vernadsky Institute, a representative ~1 g chip was crushed and powdered in an agate mortar for whole rock analysis (Table 6). The following elements were determined from a ~500 mg portion of the powder by X-ray fluorescence (XRF): Si, Ti, Al, Cr, Fe, Mn, Mg, Ca, and P. This same portion of the sample was used to determine the loss after ignition. These same elements were also determined in two ~100 mg portions of the powder by inductively coupled plasma-atomic emission spectrometry (ICP-AES). Two ~100 mg portions of the powder were used to determine Na and K by atomic absorption. Trace elements were determined in three ~20 mg portions of the powder by instrumental neutron activation analysis (INAA). A 57 mg portion of the same powder was also analyzed at UCLA; results were reported by Warren et al. (2001). Separate splits weighing ~10 mg were used to determine oxygen isotopic compositions, using the conventional techniques outlined by Clayton and Mayeda (1996).

Eight polished thin sections and probe mounts of 15418 (,8; ,10; ,18; ,19; ,26; ,98; ,155; and ,226) were examined with a petrographic microscope for comparison with Dhofar 026. One of the sections was examined with a JEOL JSM-5900 SEM and analyzed with a Cameca SX50 EMP at the University of Hawaii, using the same techniques and corrections as we used for Dhofar 026. For comparison with the bulk composition of Dhofar 026, we give a composite analysis of 15418 (Table 6). The exact location of the different analyzed subsamples of 15418 has not been well-documented, so it is not clear which analysis represents which of the zones within the rock (see below). The bulk analysis we list in Table 6 (Bansal et al. 1972) is of sawdust generated during cutting of a slab; as the bulk of the rock appears to be interior-zone material (see below), this sample should represent an average for the interior zone, with only minor admixture of material from other zones. The Bansal et al. analysis differs from other XRF major element analyses of 15418 only in FeO and MgO, resulting in a lower bulk mg# than in the other analyses. The trace-element analysis by Taylor et al. (1973) is clearly of interior-zone material (their analyzed subsample was taken near our interior-zone section 15418,98). The data for Ir, Au, and Cs (Ganapathy et al. 1973) are for a "dense interior" subsample, which was probably interior-zone material.

LUNAR METEORITE DHOFAR 026

Texture and Mineralogy

Most of Dhofar 026 consists of three textural domains: monomineralic plagioclase patches, olivine-plagioclase intergrowths, and pyroxene-plagioclase intergrowths (Fig. 1). Sparse large grains of olivine are scattered throughout the latter two domains. Locally, the rock contains small swirls, streaks, and irregular patches of brownish devitrified glass. An unusual feature of Dhofar 026 is the presence of small, sharply bounded, globular bodies consisting of intergrowths of plagioclase and mafic minerals (Figs. 1 and 2). Mass-balance calculations, normative calculations, and visual estimates indicate that ~0.5 vol% of the rock consists of globules and ~10–20 vol% consists of pyroxene-plagioclase intergrowths; the remainder consists of roughly equal amounts of olivine-plagioclase intergrowths and monomineralic plagioclase. Vesicles are common throughout the rock, especially in monomineralic plagioclase and globules. Several healed fractures are present. The bulk rock is tough, well-indurated, and unfractured.

Monomineralic Plagioclase Patches

Patches of monomineralic plagioclase have blocky outlines and are 20–300 μm across (Fig. 1). In many areas, the plagioclase is a mat of tiny acicular needles that, within the larger patches, have similar extinction. In other areas, the plagioclase consists of an intergrowth of small, complexly interpenetrating grains that contain very fine twinning. Plagioclase composition ranges from $An_{96.0}$ to $An_{98.4}$ and averages $An_{97.0}$ (Table 1; Fig. 3). Ovoid or amoeboid vesicles are common; the vesicles range from 10 to 60 μm across and average about 20 μm.

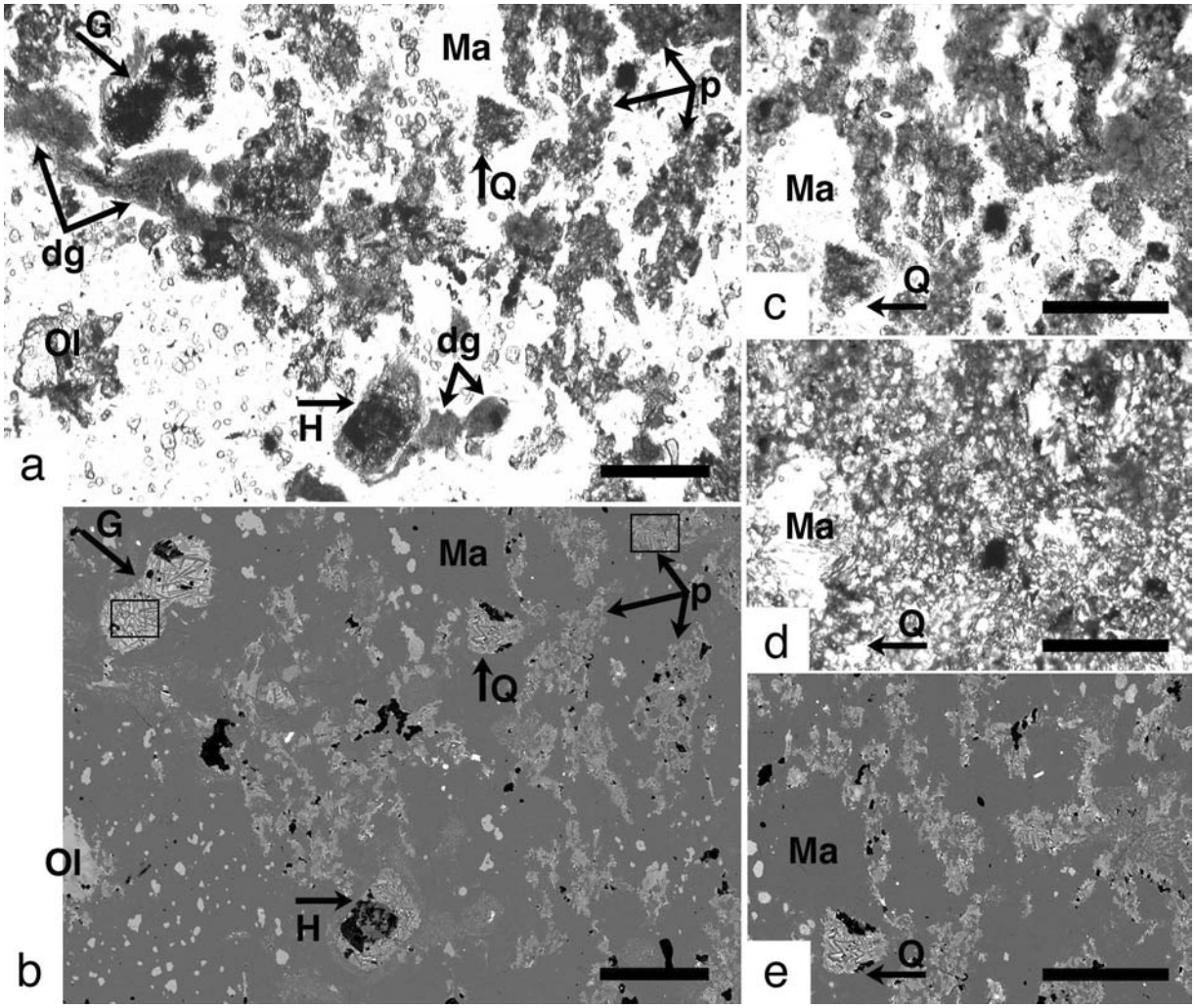

Fig. 1. Photomicrographs and BSE images of representative areas in Dhofar 026. In the BSE images, white is metal or troilite, light gray is olivine, medium gray is pyroxene, dark gray is plagioclase, and black is void space. The scale bars in all images are 200 μm: a) plane light image of a typical area; b) BSE image of the same area (except for a strip at the left edge). In olivine-plagioclase intergrowths (lower left corner; top center; below and right of center), olivine forms abundant small blebs and sparse large grains (Ol) enclosed by plagioclase. Patches of monomineralic plagioclase (Ma) are common. Pyroxene-plagioclase intergrowths form: 1) sharply bounded patches (p); and 2) highly irregular patches that fill interstices between other domains (area left of center). Intergrowths of plagioclase and mafic minerals form globules (G, H, Q). Patches and swirls of devitrified glass (dg in [a]) are common near globules. The boxes in (b) outline areas for which high-magnification BSE and X-ray images are shown in Fig. 5. Globule Q, though not studied in detail, is labeled in all images for spatial reference; c) plane light image of area near the upper right corners of (a) and (b); d) crossed-polarizer image of the same area as in (c). The plagioclase in the monomineralic patches and olivine-plagioclase intergrowths consists of a very fine acicular intergrowth; e) BSE image of the same area as in (c) and (d). Pyroxene-plagioclase intergrowths fill interstices between large blocky patches of monomineralic plagioclase (texture obscured in [c] and [d]).

Olivine-Plagioclase Intergrowths

Patches of olivine-plagioclase intergrowths have blocky or ovoid outlines and are as much as 1.5 mm across. They consist of olivine grains in a mat of extremely fine-grained acicular plagioclase and clear, devitrified, plagioclase glass (Fig. 1); the acicular plagioclase commonly forms radiating bundles of needles. Areas of plagioclase within this intergrowth contain vesicles like those in the monomineralic plagioclase patches. The olivine grains are ovoid to equant anhedral and 5–30 μm across; the larger olivine grains are mosaics of 5–10 μm subgrains that formed by recrystallization. Both olivine and plagioclase are fairly uniform in composition. Plagioclase ranges from $An_{95.1}$ to $An_{98.8}$ and averages $An_{96.5}$, slightly less calcic than that in the monomineralic patches (Table 1; Fig. 3). Olivine ranges from $Fo_{62.1}$ to $Fo_{69.4}$ and averages $Fo_{63.8}$ (Table 2; Fig. 4).

Rare elongate ilmenite grains, as much as 40 μm long, are present; the larger of these consist of 5–15 μm subgrains that are locally intergrown with armalcolite (Table 4). The ilmenite is relatively magnesian ("relict" ilmenite; Table 4).

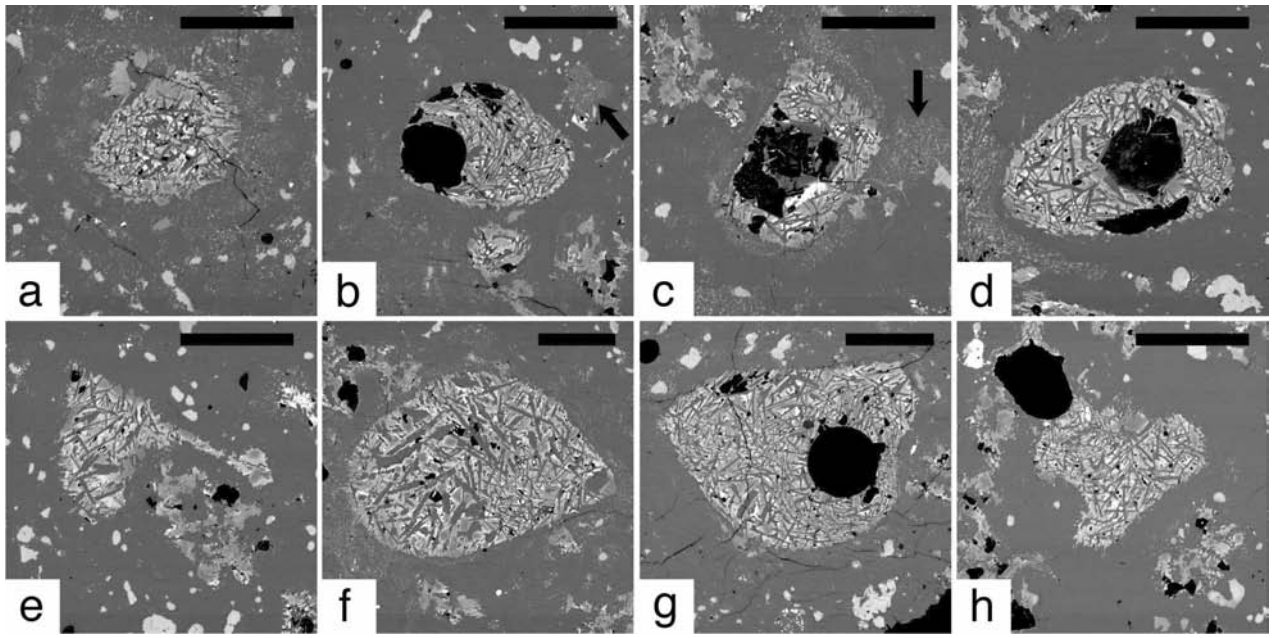

Fig. 2. BSE images of globules in Dhofar 026. The dark gray is plagioclase, the white outside the globules is olivine, the white within the globules is ferroan pyroxene and ferroan olivine, the light gray within the globules is magnesian olivine and pyroxene, the light gray outside the globules is pyroxene, and the black is void space. The scale bars are 50 μm. All globules show very fine-grained igneous textures. Plagioclase laths in the interiors of the globules are randomly oriented, indicating that the nuclei for these laths floated free in the melt: a) globule D, which is enclosed by an irregular halo of devitrified glass (finely speckled). Ferroan pyroxene is concentrated near the globule center, indicating crystallization from edge to center; b) globule E, which contains a large vesicle and has a blob of devitrified glass nearby (arrow). Globule bulk composition was determined by defocused-beam EMP analysis (Table 5); c) globule H, which has a trapezoidal outline, contains a central void, is surrounded by a thin band of devitrified glass (finely speckled light gray), and has a swirl of devitrified glass nearby (arrow). At its top right edge, the globule has a thin plagioclase rim, and small, subparallel, subhedral terminations of rim plagioclases project into the globule from the rim; d) globule I, which contains a vesicle and an elongate void. At its pointed end, the globule has a thin plagioclase rim bordered by devitrified glass (speckled); e) globule J (above left of center), a body with a long straight edge, and a patch of pyroxene-plagioclase intergrowth (below right of center). Both bodies are enclosed by olivine-plagioclase intergrowth; f) globule K, one of the largest globules. Globule bulk composition was determined by defocused-beam EMP analysis (Table 5); g) globule L, which contains a vesicle and is one of the largest globules; h) globule P, which has an amoeboid shape, one straight edge, and a vesicle at one end.

The ilmenite grains are enclosed by 10–20 μm-thick haloes in which the acicular plagioclase has interstitial slivers of mafic and oxide minerals.

Locally, the olivine-plagioclase intergrowths contain igneous-textured, ilmenite-rich patches that are 50–200 μm across. Plagioclase dominates in most of these patches; olivine dominates in only a few. The plagioclase forms tiny laths, the olivine forms small euhedra, and the ilmenite forms thin laths; pyroxene is interstitial, and in some patches, mesostasis having grain size <<1 μm fills interstices. A few patches contain irregular blebs of troilite ≤30 μm across. Ilmenite in one such patch is less magnesian than the relict ilmenite ("ilmenite crystallized from melt;" Table 4).

The bulk composition of an area of olivine-plagioclase intergrowth was determined by defocused-beam analysis (Table 5). A norm calculated from this analysis and point counts of BSE images yield an approximate mode of 90–93% plagioclase and 7–10% olivine.

Pyroxene-Plagioclase Intergrowths

Very fine-grained intergrowths of pyroxene, plagioclase, and olivine form equant, well-defined patches (Figs. 5a–5b and 2e), mostly 100–200 μm across, and irregular stringers that fill interstices between patches of the other textural domains (Fig. 1b). The margins of most intergrowths are highly irregular (Figs. 1 and 5a). Textures indicate crystallization from a melt (Figs. 5a–5b). The plagioclase, olivine, and augite form subhedral grains enclosed by subophitic-poikilitic pyroxene grains. The plagioclase laths are <15 μm long, the olivine subhedra are 5–20 μm across, the augite subhedra are ~5 μm across, and the subophitic-poikilitic pyroxene grains are optically continuous for 100–500 μm. In some intergrowths, small ilmenite needles occur within the pyroxene. An EMP X-ray map of Si concentration (not presented herein) indicates that a Si-rich phase locally forms blebs too small for quantitative analysis at pyroxene-plagioclase contacts.

As illustrated in Fig. 5a, plagioclase laths in the interior of a typical patch of pyroxene-plagioclase intergrowth are randomly oriented, indicating that the nuclei for these laths floated free in the crystallizing melt. Locally, at the margin of the intergrowth, small subparallel plagioclase laths that

Table 1. Average plagioclase compositions (wt%)[a] in Dhofar 026.

	Oliv.-plag. intergrowths	Monomineralic plagioclase patches	Globules
Number of analyses	113	23	11
SiO_2	43.8 (3)	43.7 (4)	47.9 (6)
Al_2O_3	35.0 (3)	35.2 (3)	30.2 (8)
FeO	0.32 (9)	0.23 (8)	1.20 (20)
MgO	0.17 (5)	0.14 (5)	0.97 (20)
CaO	19.4 (2)	19.6 (3)	17.8 (2)
Na_2O	0.37 (6)	0.32 (7)	0.64 (7)
K_2O	0.04 (2)	0.03 (2)	0.03 (2)
Total	99.08	99.18	98.82
Cations			
Oxygen basis	8	8	8
Si	2.046	2.039	2.235
Al	1.930	1.938	1.663
Fe	0.012	0.009	0.047
Mg	0.012	0.010	0.067
Ca	0.970	0.979	0.890
Na	0.033	0.029	0.058
K	0.002	0.002	0.002
Total	5.006	5.007	4.962
Ab	3.3	2.8	6.1
An	96.5	97.0	93.7
Or	0.2	0.2	0.2

[a] 1σ standard deviation in parentheses, expressed as error in last digit(s) of the preceding number, with decimal dropped.

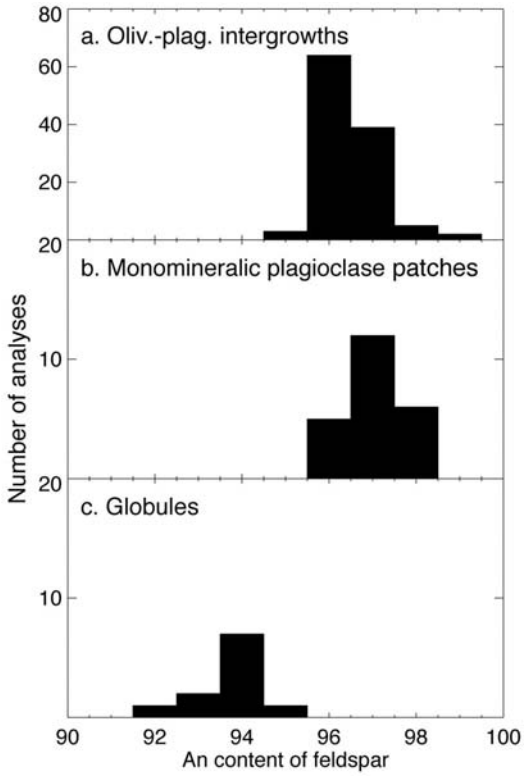

Fig. 3. Compositions of plagioclase grains (EMP analyses) in Dhofar 026; data summarized in Table 1.

project into the intergrowth are extensions of small grains at the edges of adjacent monomineralic plagioclase patches. Many other patches of pyroxene-plagioclase intergrowth show similar small marginal plagioclase laths that cross the boundary of the intergrowth into adjacent domains.

Compositional variations of the minerals in the intergrowths are consistent with crystallization from a melt. The olivine grains are normally zoned; they have a greater range of compositions ($Fo_{59.4–82.8}$), and their compositions average more magnesian ($Fo_{75.4}$) than those in the olivine-plagioclase intergrowths (Table 2; Fig. 4). Locally, magnesian low-Ca pyroxene (Table 3; Fig. 4) rims olivine, and the small subhedral augite grains are also magnesian (Table 3; Figs. 4 and 5). The poikilitic-subophitic pyroxene is more iron-rich (Table 4) and is zoned to very iron-rich compositions near grain margins (Figs. 5a–5b); unfortunately, accurate microprobe analysis of the thin marginal zones is not possible. Plagioclase laths are also too small for accurate analysis.

Olivine Grains

Scattered throughout the olivine-plagioclase and pyroxene-plagioclase intergrowths are sparse, blocky, 50–170 μm olivine grains consisting of mosaics of 5–10 μm subgrains (Fig. 1) that formed by recrystallization. These grains have compositions similar to those in the olivine-plagioclase intergrowths; their range is $Fo_{61.5–64.2}$, and their average is $Fo_{62.5}$ (Table 2; Fig. 4).

Table 2. Average olivine compositions (wt%)[a] in Dhofar 026.

	Oliv.-plag. intergrowths	Grains >50 μm	Pyrox.-plag. intergrowths	Globules, cores	Globules, rims
Number of analyses	41	12	28	9	3
SiO_2	36.3 (4)	36.2 (3)	38.0 (10)	38.1 (6)	35.0 (6)
TiO_2	0.05 (4)	0.04 (2)	0.05 (3)	0.08 (6)	0.33 (20)
Al_2O_3	0.08 (4)	0.05 (3)	0.11 (6)	0.10 (4)	0.20 (22)
FeO	31.4 (13)	32.6 (6)	22.3 (47)	20.1 (18)	37.0 (12)
MnO	0.33 (4)	0.34 (3)	0.27 (5)	0.23 (6)	0.49 (3)
MgO	31.1 (11)	30.4 (4)	38.5 (37)	40.4 (17)	25.3 (16)
CaO	0.41 (14)	0.27 (10)	0.47 (8)	0.44 (3)	0.87 (43)
Cr_2O_3	0.08 (5)	0.08 (4)	0.21 (7)	0.23 (7)	0.23 (4)
Total	99.71	100.00	99.87	99.65	99.48
Cations					
Oxygen basis	4	4	4	4	4
Si	0.993	0.994	0.991	0.987	0.991
Ti	0.001	0.001	0.001	0.002	0.007
Al	0.002	0.002	0.003	0.003	0.007
Fe	0.719	0.747	0.486	0.434	0.877
Mn	0.008	0.008	0.006	0.005	0.012
Mg	1.267	1.243	1.500	1.560	1.069
Ca	0.012	0.008	0.013	0.012	0.026
Cr	0.002	0.002	0.004	0.005	0.005
Total	3.004	3.004	3.005	3.008	2.996
Mg#	63.8	62.5	75.4	78.2	54.9

[a] 1σ standard deviation in parentheses, expressed as error in last digit(s) of the preceding number, with decimal dropped.

Contacts Between Domains

Because the plagioclase in both the monomineralic plagioclase patches and the olivine-plagioclase intergrowths consists of intergrowths of tiny acicular needles, contacts between these two textural domains cannot always be precisely determined. For example, in Fig. 1b, at the edges of the patch of olivine-plagioclase intergrowth at the lower left, there are some blocky areas of pure plagioclase that might be viewed as olivine-poor parts of the olivine-plagioclase intergrowth or as monomineralic plagioclase patches.

In some areas, it is also difficult to determine the precise location of contacts between pyroxene-plagioclase intergrowths and other domains. For example, it is commonly unclear to which domain the small blocky patches of pure plagioclase within pyroxene-plagioclase intergrowths should be assigned. The fine grain size of the rock and the thickness of the section obscure the textures within the small plagioclases, so it cannot be discerned whether they are single grains, thus crystallized from the melt that formed the pyroxene-plagioclase intergrowths, or mats of minute acicular grains, thus very small monomineralic plagioclase patches. Moreover, at the edges of pyroxene-plagioclase intergrowths, small plagioclase laths project into the intergrowths from surrounding plagioclase (Fig. 5a), so it is unclear to which domain they should be assigned. Our interpretation of the origin of the rock textures, offered herein, predicts these textural ambiguities.

Globules

Intergrowths of plagioclase and mafic minerals form globular bodies averaging 120 μm across; the smallest are about 50 μm across, and the largest is 300 × 230 μm (Figs. 1, 2, and 5). Most globules are ovoid (Figs. 2a, 2b, 2d, 2f, and 2g), but several have one or more straight edges (Figs. 2e and 2h; Q, Fig. 1e); some are amoeboid (Fig. 2h), some are blocky with rounded corners (H, Figs. 1 and 2c), and one is a composite of two globules (G, Fig. 1).

Textures indicate that the globules crystallized from melts (Figs. 5c–5d). Olivine forms euhedral, skeletal, or subophitic grains intergrown with plagioclase laths; the presence of thin plagioclase laths within the cores of the olivine grains indicates that these two phases crystallized simultaneously. Locally, pyroxene rims olivine; subophitic pyroxene and extremely fine-grained mesostasis fill interstices. Most olivine grains are 10–20 μm across, and most plagioclase laths are 10–20 μm long. Locally, the interstitial pyroxene forms microcrystalline variolitic intergrowths with plagioclase. In a few globules, pyroxene and mesostasis contain abundant ilmenite (Fig. 5c). In most globules, low-reflectivity blebs <1 μm across are concentrated along plagioclase grain boundaries, probably representing late-stage immiscible K-Si-rich melt. Vesicles are common, ranging from <1 μm (Fig. 5c) to 90 μm across (Figs. 2b, 2d, 2g, and 2h); some globules also contain vugs. None of the globules show textural disruptions that would indicate that their edges are broken surfaces. In many

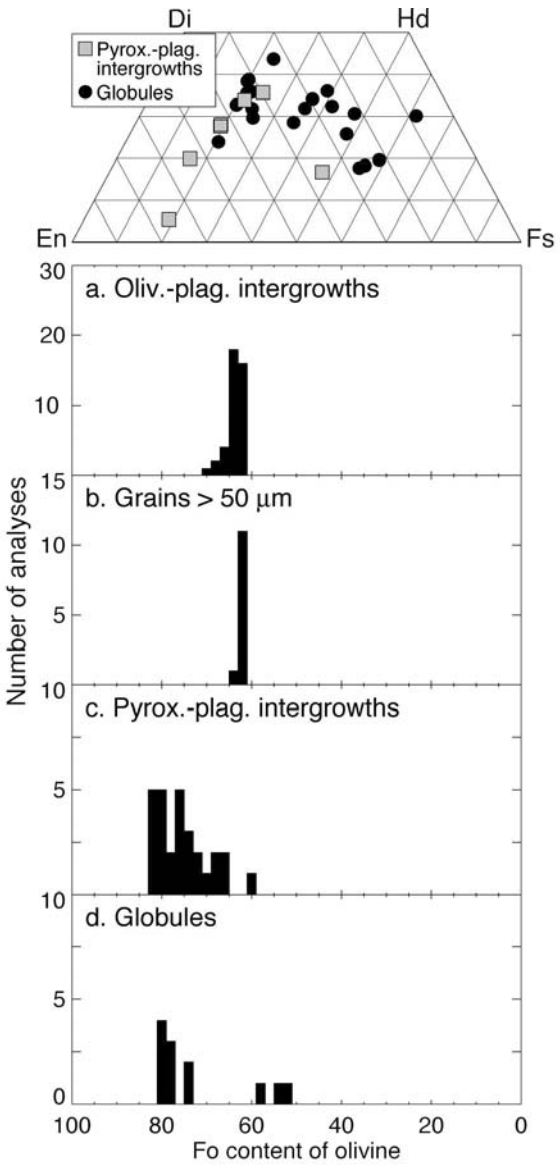

Fig. 4. Compositions of olivine and pyroxene grains (EMP analyses) in Dhofar 026; data summarized in Tables 2 and 3.

globules, olivine appears to have nucleated at the edges, and coarsening of grain size toward the globule center indicates that crystallization proceeded from the edges to the center (Figs. 2a and 2f). The minerals in the globules show no shock effects: they have uniform extinction and no shock-induced fracturing or disruption of grain outlines.

Many globules have narrow, discontinuous plagioclase rims ≤30 μm thick (Figs. 2c and 2d). Mafic minerals of the globules penetrate into interstices between rim plagioclases, and subhedral terminations of rim plagioclases project into the globules (Fig. 2c), indicating that the globules and their rims crystallized simultaneously.

The cores of olivine grains in the globules have compositions similar to those of olivines in the pyroxene-plagioclase intergrowths, ranging from $Fo_{74.5}$ to $Fo_{80.7}$ and averaging $Fo_{78.2}$ (Table 2; Fig. 4). The olivine grains are normally zoned; in one globule (G, Figs. 1 and 5c–5d), olivine rims are as iron rich as $Fo_{52.9}$ (Table 2; Fig. 4).

Pyroxene in the globules is zoned from augite, through ferroaugite, to subcalcic ferroaugite and ferrohedenbergite near grain boundaries (Table 3; Fig. 4). In a few globules, the most iron-rich pyroxene is concentrated near the center of the globule (Fig. 2a), indicating that crystallization proceeded from the edge to the center. The most magnesian augite grains are similar in composition to those in the pyroxene-plagioclase intergrowths. The most iron-rich pyroxenes are richer in iron than those analyzed in the pyroxene-plagioclase intergrowths, but the difference may only reflect the difficulty of analysis of thin edge zones.

Plagioclase in the globules is the most sodic plagioclase in the rock, ranging from $An_{92.3}$ to $An_{94.7}$ and averaging $An_{93.7}$ (Table 1; Fig. 3). The analyses show higher Mg and Fe than in the other plagioclases. Mixing calculations and evaluation of the plagioclase cation proportions by the methods of James and McGee (1992) suggest that most of the Mg and Fe are in the plagioclase structure, but we cannot rule out the possibility that some of the elevated Fe is the result of fluorescence of adjacent mafic minerals.

Table 5 presents bulk compositions of two globules, E (Fig. 2b) and K (Fig. 2f). The globules differ slightly in mg# (100 × molar Mg/[Mg + Fe]) and concentrations of TiO_2, MgO, and CaO, but both are mafic; their norms indicate they are slightly quartz normative. The presence of olivine in the actual assemblage, rather than the quartz predicted by the norm calculation, as well as the zoning of the mafic minerals and the very fine grain size, indicate geologically rapid, non-equilibrium crystallization of the globule melt.

Devitrified Glass

Irregular swirls, streaks, and blebs of cloudy, brown, devitrified glass occur throughout the olivine-plagioclase intergrowths (Fig. 1a). Such devitrified glass commonly forms discontinuous, irregular haloes around globules (Figs. 1 and 2), and blebs of glass are concentrated near globules (Fig. 1a). The devitrified glass consists of a mosaic of spherulitic plagioclase grains that contain abundant minute inclusions of mafic minerals, troilite, and perhaps voids. Bulk composition of the devitrified glass is extremely plagioclase rich.

Chromite, Sulfide, and Metal

Chromite is the most abundant oxide mineral and is found in both the olivine-plagioclase and pyroxene-plagioclase intergrowths. Chromite grains are subhedral to euhedral, are 15–35 μm across, and contain abundant minute low-reflectivity inclusions formed by partial melting. The grains are enclosed by 10–20 μm-thick haloes that consist of acicular plagioclase with interstitial slivers of mafic and oxide minerals. Chromite compositions are highly variable

Table 3. Compositions (wt%) of representative pyroxenes in Dhofar 026.

	Pyroxene-plagioclase intergrowths			Globules			
	Ortho-pyroxene	Augite	Subcalcic ferroaugite	Augite	Ferroaugite	Subcalcic ferroaugite	Ferro-hedenbergite
SiO_2	55.0	48.6	48.0	47.3	45.8	47.0	45.5
TiO_2	0.20	1.62	1.02	1.71	3.33	1.61	2.00
Al_2O_3	1.10	5.09	5.30	5.75	3.91	3.32	3.85
FeO	12.4	12.5	26.0	12.2	23.3	32.1	32.1
MnO	0.25	0.29	0.43	0.30	0.39	0.59	0.56
MgO	27.9	14.5	11.1	13.9	8.12	6.70	2.43
CaO	2.77	15.3	7.18	15.9	14.1	8.39	12.3
Na_2O	<0.03	0.06	0.11	<0.03	<0.03	0.04	<0.03
Cr_2O_3	0.57	0.52	0.08	1.58	0.10	0.04	0.03
Total	100.22	98.45	99.20	98.72	99.05	99.85	98.70
Cations							
Oxygen basis	6	6	6	6	6	6	6
Si	1.964	1.846	1.877	1.802	1.822	1.897	1.883
Ti	0.005	0.046	0.030	0.049	0.100	0.049	0.062
Al	0.046	0.228	0.244	0.258	0.184	0.158	0.188
Fe	0.370	0.396	0.852	0.388	0.777	1.084	1.112
Mn	0.008	0.009	0.014	0.010	0.013	0.020	0.019
Mg	1.483	0.821	0.646	0.791	0.482	0.403	0.150
Ca	0.106	0.623	0.301	0.650	0.604	0.363	0.544
Na	–	0.005	0.008	–	–	0.003	–
Cr	0.016	0.016	0.002	0.048	0.003	0.001	0.001
Total	3.999	3.989	3.974	3.995	3.985	3.977	3.960
Mg#	80.0	67.5	43.1	67.1	38.3	27.1	11.9
Wo	5.4	33.9	16.7	35.6	32.4	19.6	30.1
En	75.7	44.6	35.9	43.2	25.9	21.8	8.3
Fs	18.9	21.5	47.4	21.2	41.7	58.6	61.6

(Table 4): most are Ti-chromites, but we found one grain of Al-chromite. Among the Ti-chromites, Al, Mg, and Cr tend to be positively correlated and anticorrelated with Fe, Mn, and Ti.

Troilite forms small blebs within monomineralic plagioclase patches and within the plagioclase of the olivine-plagioclase intergrowths; these blebs are as large as 40 μm, but most are 1–5 μm across. Troilite composition is typical for lunar troilite, with <1% Ni (Table 4). Rare Fe-Ni metal is associated with troilite or occurs alone; the largest grains are ≤40 μm across but most are <10 μm across. The metal is typically rimmed and partly replaced by a bright red, transparent, iron-oxide mineral (hematite?). The three metal grains analyzed have highly variable Ni concentrations (Table 4).

Aberrant Textural Domains

Within the olivine-plagioclase intergrowths, several "troctolitic" patches that are 300–900 μm across have a distinctive, unusual texture. Plagioclase is acicular, as elsewhere in the intergrowths, but small olivine blebs outline what appear to be original large plagioclase laths; the olivine blebs are commonly optically continuous.

A single domain, 2 mm by 2.8 mm, with a unique texture, occurs at one edge of the section. The edge of this patch is a thick band of plagioclase, with texture similar to that in the olivine-plagioclase intergrowths; unlike elsewhere in the rock, however, the plagioclase is free of vesicles and contains abundant tiny metal and/or troilite spherules. The center of the patch is a swirled, dark-brown, cloudy intergrowth of plagioclase and mafic minerals. Part of this intergrowth has a barred texture, in which the mafic minerals form thin parallel septa between parallel plagioclase laths. In the rest of the intergrowth, mafic-mineral oikocrysts enclose ovoid plagioclase grains that contain abundant submicron inclusions of mafic minerals.

One domain, 800 by 550 μm, consists of two large patches of monomineralic plagioclase, each of which is an aggregate of subgrains having similar extinction. One of these patches contains a 180 μm equant pyroxene grain containing numerous 5–10 μm laths of plagioclase.

Healed Fractures

Three subparallel healed fractures cut across the section. One is 6 mm long, discontinuous, and marked by flattened vesicles, elongate patches of pyroxene-plagioclase intergrowths, and patches of intergrowths similar to those that make up the globules. A second fracture is 1.2 mm long and is marked by a few vesicles and elongate patches of pyroxene-plagioclase intergrowths. The third is 0.6 mm long and

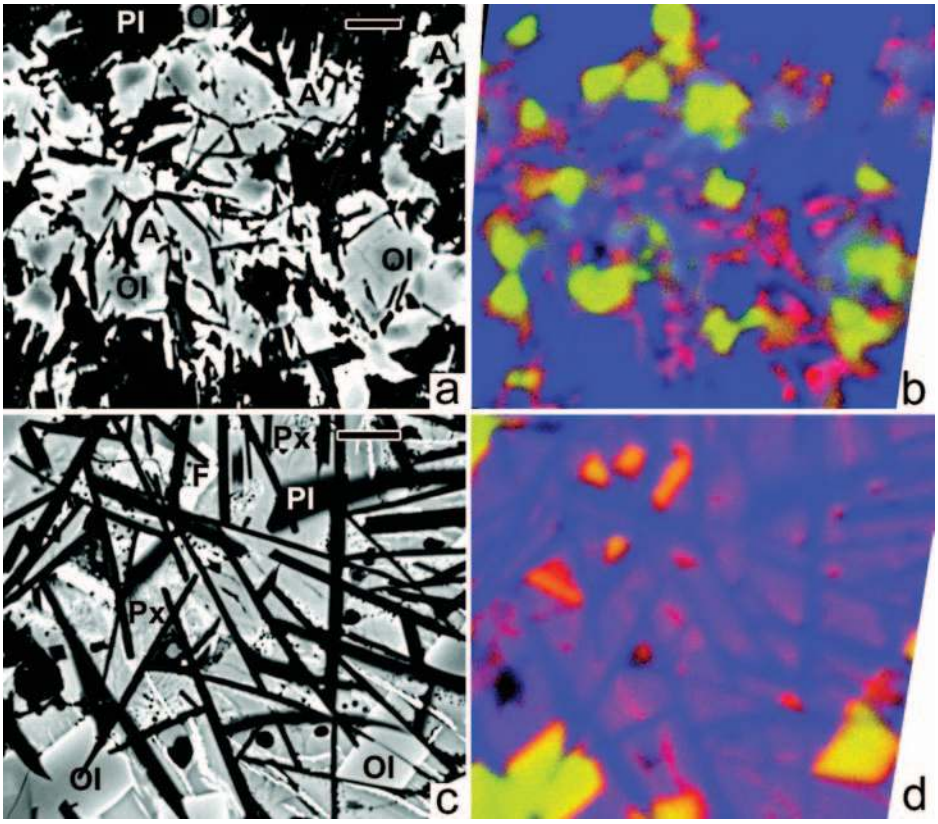

Fig. 5. BSE images and X-ray maps of pyroxene-plagioclase intergrowth and globule G (areas outlined in boxes in Fig. 1b). In the BSE images, black is void space, dark gray is plagioclase, and intermediate gray to white are pyroxenes, olivine, mesostasis, and ilmenite. The labels are as follows: Pl, plagioclase; Ol, olivine; F, iron-rich olivine (in [c] only); A, augite (in [a] only); and Px, pyroxene of unknown composition (in [c] only). The X-ray maps are three-color images in which red = Fe, green = Mg, and blue = Ca. In the X-ray maps, the colors of the phases are as follows: plagioclase, dark blue; olivine, green to yellow-green to yellow to orange; augite, pale blue; pyroxenes of increasing Fe and decreasing Ca contents, purplish blue to orange to red; ilmenite, red. Because of differing color stretches, pyroxenes of the same composition are not necessarily the same color in the two X-ray images. The scale bars are 10 μm: a) BSE image of pyroxene-plagioclase intergrowth, showing subophitic texture indicating crystallization from melt. Plagioclase laths in the interior of the intergrowth are randomly oriented, indicating that the nuclei for these laths floated free in the melt and had no preferred orientation. The margin of the intergrowth is highly irregular. Locally, at the margin, small subparallel plagioclase laths project into the intergrowth from adjacent monomineralic plagioclase patches (left of scale bar; bottom left corner). The subparallel orientation of these marginal laths indicates that they nucleated on, and their orientation was determined by, the crystal structure of adjacent plagioclase; b) X-ray map of the same area as (a). Euhedral-subhedral olivine and augite are enveloped by subophitic pyroxene; c) BSE image of globule G. The presence of thin laths of plagioclase within the magnesian cores of the olivine indicates that these two phases crystallized simultaneously. Pyroxene and mesostasis fill interstices. Needles of ilmenite occur in pyroxene and mesostasis, and small vesicles are abundant in mesostasis. Small euhedra of iron-rich olivine (F) are present; d) X-ray map of same area as (c). Euhedra of magnesian olivine have iron-rich rims.

consists of a 20 μm band of intergrowths of plagioclase and mafic minerals similar to those within globules.

Bulk Composition

Enrichments in Sr, Ba, K, Ca, As, Br, Sb, and Cs are characteristic of weathering of meteorites in hot desert environments (Bischoff et al. 1998; Korotev et al. 2003; Nazarov et al. 2003). The Sr (200 ppm; Table 6) and Ba (56 ppm; Warren et al. 2001) concentrations in our samples of Dhofar 026 indicate relatively little terrestrial weathering in comparison to Dar al Gani (DaG) 262, another lunar feldspathic meteorite found in a hot desert (Sr = 245 ppm, Ba = 240 ppm; Bischoff et al. 1998). The K_2O concentration, however, is 2–3 times greater than in feldspathic lunar meteorites from Antarctica that have similar REE concentrations (Korotev et al. 2003), and the Cs in the sample appears largely to be terrestrial contamination (Korotev, personal communication). The Au concentration in the bulk rock is high, and the Au-Ni ratio is much higher than in most feldspathic lunar meteorites (Korotev et al. 2003) or in lunar rocks of bulk composition like that of Dhofar 026 (Table 6), indicating significant terrestrial Au contamination. Although our sample appears to be relatively unweathered, other samples of Dhofar 026 appear to have experienced more extensive terrestrial weathering (Warren, personal communication).

Dhofar 026 has a gabbroic-anorthosite bulk composition (Table 6), similar to that of other feldspathic lunar meteorites

Table 4. Compositions (wt%) of oxides, metal, and sulfide in Dhofar 026.

	Oxide minerals						Metal	Troilite
	Ilmenite, relict	Ilmenite, crystallized from melt	Armalcolite	Al-chromite	Ti-chromite			
Number of analyses	1	1	1	1	8	Number of analyses	3	1
SiO_2	0.05	0.11	0.16	0.07	0.21–0.09	Fe	68.1–80.7	61.8
TiO_2	55.5	54.0	69.1	5.23	13.2–21.3	Co	1.01–1.35	<0.03
Al_2O_3	0.38	0.21	4.52	11.3	12.3–6.77	Ni	15.4–26.6	0.53
FeO	32.4	35.2	15.6	27.4	31.5–40.1	S	<0.03–0.29	36.3
MnO	0.32	0.26	0.14	0.18	0.16–0.37	P	<0.03–0.03	<0.03
MgO	8.34	6.60	6.28	6.29	8.05–5.57	Si	0.04–0.28	0.05
CaO	0.29	0.65	0.37	0.29	0.49–0.27	Total	96.09–97.96	98.69
Cr_2O_3	1.15	0.59	0.81	47.4	34.5–23.6			
Total	98.44	97.63	97.04	98.10	97.93–98.68			
Cations								
Oxygen basis	3	3	5	4	4		Mole percent	
Si	0.001	0.003	0.006	0.003	0.003–0.007		Fe	48.5
Ti	0.996	0.993	1.909	0.135	0.336–0.545		Co	–
Al	0.011	0.006	0.195	0.454	0.490–0.277		Ni	0.39
Fe	0.647	0.720	0.480	0.783	0.889–1.151		S	49.7
Mn	0.007	0.005	0.004	0.005	0.005–0.011		P	–
Mg	0.296	0.240	0.344	0.321	0.403–0.285		Si	0.07
Ca	0.007	0.017	0.014	0.011	0.018–0.010		Total	98.69
Cr	0.022	0.011	0.024	1.283	0.921–0.641			
Total	1.987	1.996	2.976	2.994	2.963–2.999			
Mg#	31.4	25.0	41.7	29.1	19.9–30.9			

(e.g., Bischoff et al. 1998; Palme et al. 1991; Zipfel et al. 1998; Korotev et al. 2003), lunar ferroan granulitic breccias (Table 6), and some lunar feldspathic impact-melt rocks (Table 6). Like other feldspathic lunar meteorites, Dhofar 026 has a prominent positive Eu anomaly ($[Eu/Sm]_{sample}/[Eu/Sm]_{chondritic}$ = 1.5–2.6). The Sc and Sm concentrations of the meteorite and its Ti/Sm fall in the middle of the ranges shown by the other feldspathic lunar meteorites, but its Al_2O_3 concentration is higher, and its mg# is lower, than in the other meteorites (Figs. 6–7). The concentrations of most siderophile elements in Dhofar 026 fall within the range reported for lunar highland meteorites (Bischoff et al. 1998; Palme et al. 1991) and are much higher than in lunar pristine rocks such as ferroan anorthosite 60025 (Table 6), indicating the presence of a significant meteoritic component.

Warren et al. (2001) presented a bulk analysis of Dhofar 026 that agrees with our analysis with a few exceptions, most notably Mg, Ir, and Ir/Au. The explanation for these differences is unclear because our samples and the Warren et al. (2001) sample were all splits from the same powder.

Origin and History

Evidence for Lunar Provenance

Many characteristics of Dhofar 026 indicate it is a lunar rock and cannot be a terrestrial rock or a plagioclase-rich eucrite or shergottite. The bulk composition (Table 6) and anorthitic plagioclase are typical of lunar highlands rocks in which ferroan anorthosite (FAN) is a major component. The bulk Fe-Mn ratio (68) is in the middle of the range for feldspathic lunar rocks (~60–80; Palme et al. 1991), significantly higher than in shergottites or eucrites (<60; Palme et al. 1991). Dhofar 026 has $\delta^{18}O$ = +5.77‰ and $\delta^{17}O$ = +2.87‰ (Taylor et al. 2001); this oxygen-isotopic composition lies on the terrestrial fractionation line (Fig. 8) and is consistent with those reported for all other lunar meteorites (Bischoff et al. 1998; Clayton and Mayeda 1996; Fagan et al. 2002).

Evidence for Pervasive Shock

The texture of the plagioclase in Dhofar 026 provides evidence that the rock was subjected to pervasive shock. The fine acicular subgrains that make up many of the larger patches of monomineralic plagioclase have similar extinction, indicating preservation of a pre-existing crystal structure. Many patches of monomineralic plagioclase have blocky outlines, indicating preservation of the shapes of pre-existing grains. Because the patches are monomineralic, they must represent a glass or melt of pure plagioclase. These characteristics indicate that the plagioclase is devitrified maskelynite (shock-generated plagioclase glass). Furthermore, the textures of the plagioclase in the

Table 5. Bulk compositions (wt%)[a] of materials in Dhofar 026 (from defocused-beam EMP analyses).

	Oliv.-plag. intergrowth uncorrected	Globule K uncorrected	Globule K corrected[b]	Globule E uncorrected	Globule E corrected[b]
Number of analyses	35	11		5	
SiO_2	43.0 (6)	49.8 (27)	49.7	48.7 (6)	48.4
TiO_2	0.04 (3)	1.20 (56)	1.32	2.40 (43)	2.67
Al_2O_3	32.4 (17)	15.2 (54)	13.7	16.8 (32)	15.3
Cr_2O_3	0.03 (3)	0.30 (13)	0.33	0.30 (16)	0.33
FeO	3.36 (199)	11.8 (40)	12.8	11.6 (22)	12.7
MnO	0.04 (3)	0.22 (8)	0.24	0.19 (7)	0.22
MgO	2.47 (162)	9.05 (628)	9.83	5.53 (186)	6.05
CaO	17.6 (12)	12.7 (28)	12.4	14.5 (15)	14.1
Na_2O	0.37 (4)	0.29 (12)	0.25	0.37 (13)	0.33
K_2O	0.04 (1)	0.03 (1)	0.03	0.07 (4)	0.06
P_2O_5	0.03 (7)	0.03 (4)	0.03	<0.03 (3)	<0.03
Total	99.39	100.51	100.71	100.41	100.11
Mg#	57	58	58	46	46
Mineral norm (weight)					
Ap	0.07	0.07	0.07	–	–
Cm	0.04	0.44	0.49	0.44	0.49
Il	0.08	2.28	2.51	4.56	5.07
Feldspar	89.7	42.7	38.6	47.5	43.1
Or	0.24	0.18	0.18	0.41	0.35
Ab	2.86	2.45	2.12	3.13	2.79
An	86.6	40.1	36.3	44.0	40.0
Di	0.41	18.7	20.7	23.3	25.0
Hy	–	33.1	35.8	19.6	21.7
Ol	8.91	–	–	–	–
Q	–	3.25	2.55	5.07	4.75
Ne	0.15	–	–	–	–
Pyroxene	0.41	51.9	56.5	42.9	46.7
Wo	50	18	18	27	27
En	28	49	49	37	37
Fs	22	33	33	36	36
Plagioclase An	96	94	94	93	93

[a] 1σ standard deviation in parentheses, expressed as error in last digit(s) of the preceding number, with decimal dropped.

[b] Corrections using the procedure of Warren (1997). Data are as follows: plagioclase composition, analysis 3, Table 1; pyroxene composition, analysis 5, Table 3; olivine composition, analysis 4, Table 2; plagioclase density, 2.76; pyroxene density, 3.47; olivine density, 3.45; globule E, 9% olivine, 41% pyroxene, 50% plagioclase, initial bulk density 3.08, iterated bulk density 3.12; globule K, 8% olivine, 48% pyroxene, 44% plagioclase, initial bulk density 3.11, iterated bulk density 3.15.

monomineralic patches and the olivine-plagioclase intergrowths are identical to, though finer grained than, textures produced by devitrification of maskelynite in 15418 (see below). Thus, the textures indicate that nearly all the plagioclase in the monomineralic patches and olivine-plagioclase intergrowths is devitrified maskelynite (the exception is the plagioclase in the sparse, small, igneous-textured, ilmenite-rich patches in the olivine-plagioclase intergrowths; these patches crystallized from melt).

Recently, controversy has developed over the definition of the term "maskelynite" and the origin of this type of plagioclase glass. Clearly, such glass formed as the result of shock, but the exact nature of the process that transforms the plagioclase to glass and the shock pressure required for the transformation are controversial (Chen and El Goresy 2000; Stöffler 2000). Herein, we will use the term "devitrified maskelynite" for the devitrified, shock-generated plagioclase glass in Dhofar 026 with the caveat that we cannot specify the exact nature of the shock-induced transition that converted the plagioclase to glass (the nature of this process is not important to our interpretation of the history of the rock).

Evidence for In Situ Post-Shock Crystallization of Pyroxene-Plagioclase Intergrowths and Globules

Textures and mineral-compositional variations within the pyroxene-plagioclase intergrowths establish that these intergrowths are not clasts but crystallized in situ, after the shock event. Evidence that the intergrowths are not clasts is as follows: 1) the intergrowths do not have sharp contacts with

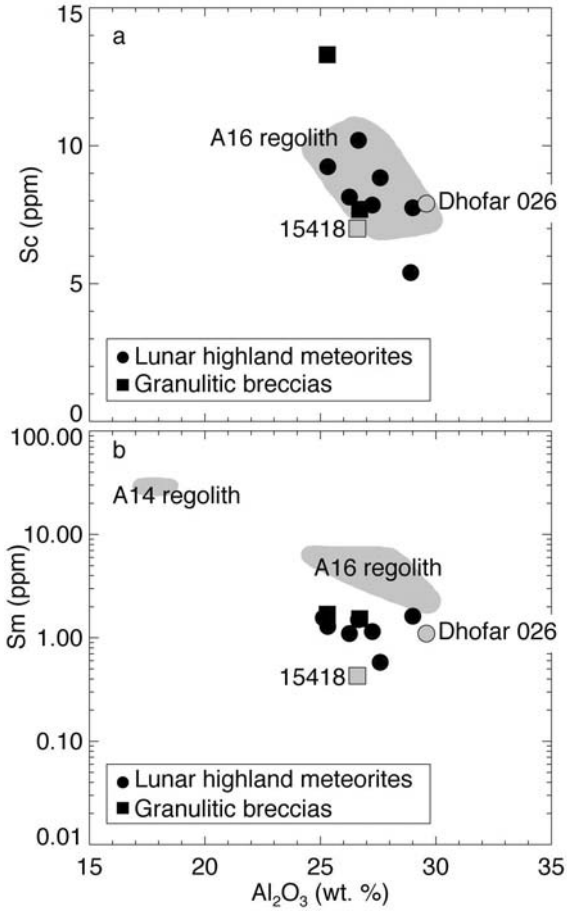

Fig. 6. Sc and Sm versus Al_2O_3 in feldspathic lunar meteorites, lunar granulitic breccias, and regolith from Apollo highlands landing sites. Data for lunar meteorites (MAC 88104, ALH A81005, Y-86032, Y-791197, QUE 93069, DaG 262, DaG 400, and Dhofar 025) are from Korotev et al. (1996), Palme et al. (1991), Taylor et al. (2001), and Zipfel et al. (1998). The compositional envelopes of Apollo 14 and 16 regoliths (Korotev, personal communication) are shown for reference. The compositions of lunar granulitic breccias are those given in Table 6: a) Sc versus Al_2O_3; b) Sm versus Al_2O_3.

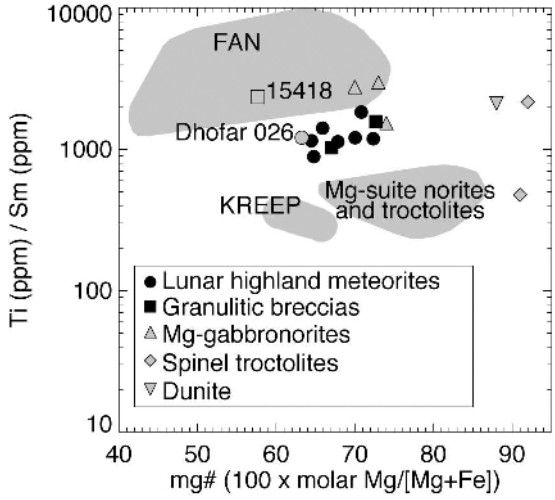

Fig. 7. Ti/Sm versus mg# (100 × molar Mg/[Mg + Fe]) in feldspathic lunar meteorites, lunar granulitic breccias, and lunar pristine rocks. The data sources for the lunar meteorites are the same as in Fig. 6; compositions of granulitic breccias are given in Table 6. The fields for lunar pristine rocks are from Taylor (1982), modified by adding data from James et al. (1989) and James and Flohr (1983). The compositional fields for pristine rocks are as follows: ferroan anorthosites (FAN); Mg-suite norites and troctolites; and KREEP basalts (KREEP). Individual points are shown for Mg-suite gabbronorites, Mg-suite dunite, and Mg-suite spinel troctolites.

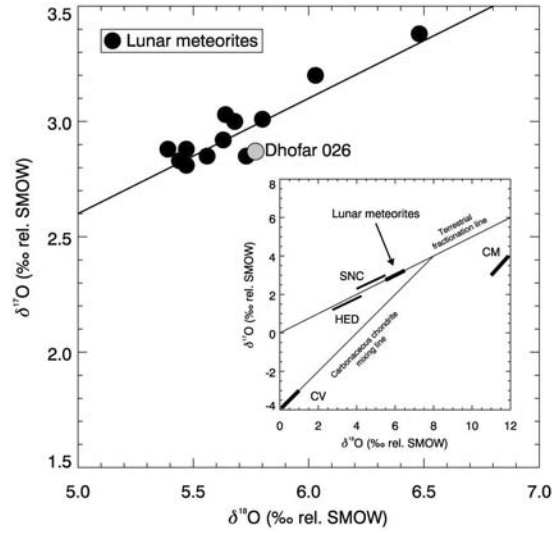

Fig. 8. Oxygen isotopic compositions of Dhofar 026, other lunar meteorites, and other meteorite groups. The other meteorite groups are as follows: SNC, shergottite-nakhlite-chassignite meteorites, thought to be from Mars; HED, howardite-eucrite-diogenite meteorites; and CV and CM, two groups of carbonaceous chondrites. Data from Taylor et al. (2001), Clayton and Mayeda (1996), Fagan et al. (2002), and Zipfel et al. (1998).

their surroundings; 2) many intergrowths are highly irregular in outline and penetrate, locally on a very fine scale, into and between patches of monomineralic plagioclase and olivine-plagioclase intergrowth (Figs. 1b and 1e); and 3) pyroxene grains within the intergrowths are zoned toward their margins, and there are none of the broken edges that would be expected if these were clasts. The absence of shock-induced disruption of grain outlines within the pyroxene-plagioclase intergrowths indicates that these intergrowths were not subjected to the shock that affected the bulk of the rock; thus, the intergrowths must have crystallized after the shock.

One of the strongest lines of evidence for post-shock crystallization is the observation that some small plagioclase laths at the edges of the intergrowths grew as extensions of plagioclase grains formed by devitrification of maskelynite bordering the intergrowths. As illustrated in Fig. 5a, at the margin of many pyroxene-plagioclase intergrowths, small plagioclase laths that project into the intergrowth have subparallel orientations; these orientations are the same as those of crystallites in the adjacent devitrified maskelynite. The orientations of these plagioclase laths indicate that their crystal structures were determined by the crystal structures of

Table 6. Whole-rock analyses of Dhofar 026 and similar lunar rocks.

Oxide (wt%)	Dhofar 026	Dhofar 026 1σ error (% of amount present)	Ferroan anorthosite 60025[a]	Granulitic breccia 15418[b]	Granulitic breccia 78155[c]	Granulitic breccia 79215[d]	Feldspathic impact melt 68415-6[e]
SiO_2	44.3	1	45.3	44.2	45.4	43.5	45.4
TiO_2	0.22	14	<0.02	0.27	0.29	0.4	0.32
Al_2O_3	29.6	0.7	34.2	26.6	25.3	26.7	28.6
Cr_2O_3	0.08	15	<0.01	0.11	0.14	0.12	0.14
FeO	4.06	3	0.50	6.65	5.63	4.91	4.25
MnO	0.06	15	0.01	0.08	0.09	0.06	0.05
MgO	3.92	3	0.21	5.08	6.42	7.33	4.38
CaO	17.0	0.7	19.8	16.0	15.2	15.6	16.4
Na_2O	0.24	0.5	0.45	0.27	0.38	0.56	0.41
K_2O	0.08	0.5	0.11	0.01	0.07	0.11	0.06
P_2O_5	0.05	15	<0.01	0.03			0.06
LOI[f]	0.57	1					
Total	100.18		100.58	99.30	98.92	99.29	100.07
Ti/Sm	1200			2350	1030	1570	621
Mg#	63.3		42.8	57.7	67.0	72.7	64.8
Element (ppm)							
Sc	7.9	4	0.7	7.0	13.3	7.69	8.38
Co	13.6	4	0.73	10	14.3	16.6	13.5
Ni	170	9	1.1	54	80	255	137
Sr	200	10	231	140	141		184
Zr	32	15	0.51		54		113
Cs	0.44	15	0.002	0.008	0.11	0.005	0.09
La	2.9	3	0.28	1.07	4.28	3.3	7.54
Ce	6.6	5	0.65	3.31	11.3	9.1	19.6
Nd	3.8	10	0.42	2.09	7.3		12
Sm	1.1	2	0.092	0.69	1.69	1.53	3.45
Eu	1.1	2	1.04	0.73	0.86	0.77	1.13
Tb	0.25	7	0.20		0.39	0.34	0.70
Yb	0.85	5	0.048	0.74	1.83	1.5	2.50
Lu	0.15	5	0.006	0.12	0.271	0.23	0.343
Hf	0.86	6	0.017	0.16	1.49	1.1	2.61
Ta	0.24	9			0.25		0.3
Ir[g]	6.3	5	0.006	2.2	3.9	21.3	4.58
Au[g]	9	5	0.007	0.26	0.68	8.27	2.65
Th	0.36	6		0.10	0.84	0.37	1.23

[a]Majors, most trace: Haskin et al. 1973; Cs, Ir, Au: Krähenbühl et al. 1973; Zr, Hf: Ehmann et al. 1975; Sr: Nyquist et al. 1975.
[b]Majors, REEs, Sr: Bansal et al. 1972; Mn, Cr, P: Lunar Sample Preliminary Examination Team 1972; Ir, Au, Cs: Ganapathy et al. 1973; all others: Taylor et al. 1973.
[c]Wänke et al. 1976.
[d]Majors, REEs, Sc, Co, Hf: Blanchard et al. 1977; Ni, Ir, Au, Cs: Higuchi and Morgan 1975.
[e]Majors: Hubbard et al. 1974 and Bansal et al. 1972; Mn, Cr, P: Rose et al. 1973; Ir, Au: Krähenbühl et al. 1973; all others: Korotev 1994.
[f]Losses after ignition.
[g]ppb.

the adjacent plagioclase; thus, they must have nucleated on the adjacent plagioclase (the reverse cannot be the case because the adjacent plagioclase is devitrified maskelynite, and the orientation of crystallites in devitrified maskelynite is determined by the structure of the original crystal). The orientation of the small laths at the margins of the pyroxene-plagioclase intergrowths can only have been affected by the structure of adjacent plagioclase if the adjacent plagioclase was crystalline when the plagioclase laths precipitated. If the intergrowths crystallized before the shock event, they should show shock effects, but they do not. Thus, the intergrowths must have crystallized after the shock event and during or after devitrification of the shock-generated maskelynite.

There are no shock effects observed in the minerals of the globules; thus, the globule melts must also have crystallized after the shock that affected the bulk rock. Moreover, many of the globules show textures that indicate in situ crystallization. Many globules are enveloped by plagioclase rims that appear

to have nucleated on surrounding plagioclase, indicating that the rims formed in situ. In the globules that have plagioclase rims, the plagioclase within the globule crystallized at the same time as the rim plagioclase (Fig. 2c). If the rims crystallized in situ, then the crystallization of the globule also must have been in situ. Some of the large vesicles that formed during globule crystallization are positioned such that they must have formed after the globule was incorporated into the rock (e.g., Fig. 2h). In some globules, olivine appears to have nucleated first at the globule margin, and in some, pyroxene zoning (Fig. 2a) or coarsening of grain size toward the center of the globule (Fig. 2f) indicates that crystallization proceeded inward from the globule margin (Fig. 2a).

Evidence that Dhofar 026 is a Shocked Rock, Not a Shock-Generated Impact Melt

Cursory examination of the texture suggests that the rock might be a clast-laden impact melt, with the devitrified maskelynite and olivine-plagioclase intergrowths representing strongly shocked clasts and the pyroxene-plagioclase intergrowths representing crystallized impact melt (the term "impact melt," as used herein and by most other investigators, refers to rock in which the melt fraction formed by shock-induced fusion). However, detailed examination of the overall texture indicates that this interpretation is unlikely. Clasts incorporated in impact melts generally show a wide range of shock effects, most show low degrees of shock, and only a small proportion are strongly shocked (Simonds 1975; Grieve et al. 1974; James et al. 1975; James 1976). Also, if Dhofar 026 were an impact melt with such a large proportion of clastic material (≥80%), we would expect: 1) the melt to have been quenched by the clasts so that it could not penetrate the clastic material on a fine scale; and 2) clast boundaries to be well-preserved. Thus, the pervasive, uniform, strong shock effects and the absence of well-defined clast boundaries indicate that the sample is a shocked rock, not a clast-laden impact melt. Accordingly, the melts that crystallized after the shock, to form the pyroxene-plagioclase intergrowths and globules, must have formed by post-shock partial melting within the rock. The haloes around relict ilmenite and chromite grains and the unshocked, igneous-textured, ilmenite-rich patches in olivine-plagioclase intergrowths must also represent local post-shock partial melts (multiphase areas containing oxide minerals would have had lower melting temperatures than areas consisting only of olivine and plagioclase). The sieve texture of the chromite grains also formed during the partial melting. The plagioclase rims on the globules formed as plagioclase dissolved in the globule melts precipitated on plagioclase surrounding the globules.

At first glance, the observation that the olivine within the pyroxene-plagioclase intergrowths is more magnesian than the relict olivine appears inconsistent with a partial-melting origin of the intergrowths; we might expect that a partial melt would have a lower mg# than the bulk rock and, thus, crystallize olivine that is more ferroan than relict olivine. In 15418, however, we observe that, as in Dhofar 026, olivine that is in contact with melt produced by post-shock partial melting is more magnesian than relict olivine (see below). Further consideration of phase petrology suggests an explanation of the relatively magnesian olivine compositions. In equilibrated rocks in which olivine has an mg# lower than about 80, olivine is more ferroan than coexisting orthopyroxene; the more ferroan the olivine, the greater the difference between the olivine and orthopyroxene (Grover and Orville 1969). In addition, in equilibrated rocks, the mg# of augite is generally higher than that of orthopyroxene (Grover and Orville 1969). Sample 15418 shows these relationships well: the mg# of relict olivine is ~55, that of relict orthopyroxene is ~65, and that of relict augite is ~72 (Nord et al. 1977). In Dhofar 026, no relict pyroxene is preserved, but data presented by Grover and Orville (1969) indicate that orthopyroxene and augite in equilibrium with the relict olivine (mg# = 63) would have been more magnesian than the olivine (mg# ~68 and ~75, respectively). Partial melting of Dhofar 026 would have begun in multiphase areas consisting of pyroxenes + plagioclase + olivine (±oxide minerals) because these areas had the lowest melting temperatures. Because of the abundance of pyroxene in such areas, the areas would have had higher mg# than the bulk rock. In areas of partial melting, the first melt would have consisted of pyroxenes + plagioclase, and olivine would have been the last phase melted. As melting proceeded, the last of the orthopyroxene to be melted would have reacted to olivine + melt, so the proportion of olivine in areas experiencing partial melting would increase until all the pyroxene was melted. The unmelted olivine within the melt would have become depleted in Fe and enriched in Mg by diffusive exchange with the melt (such diffusive exchange is clearly shown in 15418; see below). The observation that there was no melting at olivine-plagioclase contacts elsewhere in the rock indicates that most of the olivine in the partially melted areas did not melt. Crystallization of the melt was rapid and non-equilibrium, as indicated by the strong zoning of the pyroxene. The rapid crystallization formed shells of pyroxene around the olivine and prevented diffusive exchange between the olivine and the melt during crystallization; thus, the relatively high mg# of the olivine, produced by earlier diffusive exchange, was preserved. In addition, the rapid crystallization prevented some of the olivine from reacting with melt to form orthopyroxene so that, at the end of crystallization, minor excess Si remained in the melt and Si-rich minerals (or glass) precipitated in interstices (visible in Si X-ray images).

Post-Shock Thermal History

We have estimated the post-shock temperature of the rock using the MELTS programs (Ghiorso and Sack 1995)

and MAGPOX (Longhi, personal communication; valid only for compositions in which olivine is a liquidus phase). The low oxygen fugacity of the rock was approximated as follows: in the MAGPOX calculation, the Fe_2O_3 concentration of the composition considered was set at 0 wt%; and in the MELTS calculations, oxygen fugacity was set at the iron-wüstite buffer. Because the post-shock temperature of the rock was high enough to melt all the original pyroxene but not all the olivine, the temperatures at which these two minerals would have been dissolved into partial melt should bracket the post-shock temperature. MELTS calculations indicate that, in a partial melt of the bulk Dhofar 026 composition, all pyroxene would have been melted at 1175 °C and all olivine at 1230 ºC. In addition, calculated temperatures at which the two globules we analyzed (E and K; Table 5) would be entirely melted set lower limits on the post-shock temperature (because the silicate fractions of these globules were entirely melted, the bulk rock should have been at least as hot as their melting temperatures). The calculated temperature at which the silicate fraction of globule E (corrected composition; Table 5) would be entirely melted is 1208 °C (MELTS), and the corresponding temperature for globule K (corrected composition; Table 5) is 1217–1212 °C (MELTS and MAGPOX, respectively). These calculated temperatures are only rough estimates, however, because of the considerable uncertainties in the defocused-beam analyses and the correction procedures. Taken together, all these results suggest that post-shock temperature of the bulk rock was about 1200 °C.

An estimate of post-shock temperature derived directly from crystallization experiments is slightly higher. Crystallization experiments were carried out at low oxygen fugacities on the composition of feldspathic melt rock 68415 (Walker et al. 1973), a rock similar in bulk composition to Dhofar 026 (Table 6). These experiments indicated that, at low pressures, all pyroxene should have been incorporated into the partial melt at about 1250 °C. (The low pressure data are used because most of the melting should have taken place after release of the shock pressure.)

Estimates of Shock Pressure and Predicted Post-Shock Temperature

Estimates of equilibrium shock pressures in shocked rocks are generally based on the results of shock experiments. Recent studies, however, have suggested that shock experiments may not duplicate shock processes occurring in natural impacts (Chen and El Goresy 2000; DeCarli et al. 2002; Sharp et al. 2003). Natural shocks will probably have longer pressure pulses than those attainable in laboratory experiments; thus, in natural shocks, kinetic effects may become important. Current studies are attempting to model the effects of longer pressure pulses (e.g., Sharp et al. 2003), and the results may necessitate revision of the currently accepted correlations between shock effects and shock pressures (e.g., Stöffler et al. 1991). Many decades of study of naturally shocked materials, however, have established the sequences of shock effects that are produced in minerals by increasing shock pressures, as well as the correlations of these shock effects among minerals. Revision of the absolute values of shock pressures will not necessitate revision of these sequences or correlations.

With the above caveat, we will estimate equilibrium shock pressure for the bulk rock using experimental data on shock effects in plagioclase (summarized by Stöffler et al. [1988, 1991]). Plagioclase shock effects are as follows: no effects at pressures less than ~5 GPa; fracturing between ~5 and ~30 GPa; mosaic extinction and planar deformation features between ~20 and ~30 GPa; conversion to maskelynite above ~30 GPa; conversion to "normal" glass (glass that retains little or no memory of the pre-existing crystal structure and contains vesicles and flow features) at ~42–45 GPa; and mixing of the "normal" glass with shock-generated melts of mafic minerals above ~80 GPa. Whole rock shock melting takes place at pressures above ~100 GPa.

Recrystallization experiments conducted on maskelynites are also relevant to the post-shock thermal history of Dhofar 026. Under normal conditions, maskelynite cools rapidly after it forms and does not devitrify. Ostertag and Stöffler (1982) found that experimentally produced maskelynite devitrified if it was reheated to temperatures higher than ~900 °C; Mikouchi et al. (2002) found the same result for natural maskelynite. At reheating temperatures of 1000 °C, Ostertag and Stöffler (1982) found that maskelynite formed at pressures between 30 and 40 GPa devitrified into aggregates of tiny subgrains with orientations close to those of the original grains, and maskelynite formed at 45 GPa devitrified into a coarse spherulitic aggregate. In both studies, small vesicles formed in the maskelynites during devitrification.

The textures of the Dhofar 026 plagioclase indicate that it is devitrified maskelynite. Thus, equilibrium shock pressure for the bulk rock must have been above 30 GPa but no higher than 45 GPa. If shock pressure had been much above 45 GPa, most of the glass should have been "normal" glass, and the glass should have flowed during the shock pulse, disrupting the relict texture.

However, this estimate of shock pressure based on plagioclase is not consistent with estimates based on shock effects in mafic minerals. At pressures between 30 and 45 GPa, olivine should show planar fractures, planar deformation features, and mosaicism, and pyroxene should show mechanical twinning, shock-induced mosaicism, and planar deformation features (Stöffler et al. 1991). Olivine begins to recrystallize at about 45 GPa, but neither phase should begin to melt until shock pressures exceed ~75 GPa. In addition, the estimate of post-shock temperature derived above, ~1200 °C, is not consistent with the post-shock temperature expected for shock pressures of 30–45 GPa. At such pressures, post-shock

temperature should be no more than 900 °C higher than pre-shock temperature, not high enough to produce the observed melting of pyroxene, recrystallization of olivine, and devitrification of maskelynite (Ostertag and Stöffler 1982).

The discrepancy between post-shock temperature estimates derived from plagioclase and mafic minerals can be resolved if the rock experienced heating in addition to that generated by the shock pressure pulse. There are several likely sources for such heating. Before the shock, the rock could have been at an elevated temperature. During the shock, the rock could have been injected by hot impact melt. After the shock, the rock could have been buried by hot ejecta or enveloped in hot impact melt. That the rock was injected by hot impact melt appears likely: Paul Warren (personal communication) reports that a lunar meteorite from Oman that is paired with Dhofar 026 contains thick veins of impact melt. We cannot rule out the possibility, however, that the rock was enveloped by impact melt in addition to having been injected by such melt.

Evidence for the Pre-Shock Nature of Dhofar 026

The overall texture of Dhofar 026 indicates that the bulk of the rock was originally granulitic breccia. The similarity to granulitic breccias is most evident in BSE images (Fig. 9). The overall texture is like that typical of poikilitic-granoblastic granulitic breccias (Cushing et al. 1999): the olivine-plagioclase intergrowths in Dhofar 026 correspond to granoblastic areas in poikilitic-granoblastic breccias; the monomineralic plagioclase patches correspond to plagioclase grains; and the pyroxene-plagioclase intergrowths correspond to poikilitic areas. Shapes of the olivine grains in the olivine-plagioclase intergrowths are especially diagnostic. The ovoid to equant anhedral shapes of the olivine grains are identical to those in granoblastic areas of granulitic breccias; such grain shapes are typical of recrystallized rocks (Cushing et al. 1999; James and Hammarstrom 1977). The overall texture of the original granulitic breccia has been mostly preserved, with post-shock melting localized in the poikilitic areas (areas with the lowest melting temperatures). The similarity of the overall texture to that of granulitic breccias further reinforces our conclusion that Dhofar 026 is not an impact melt breccia.

The areas of Dhofar 026 described above as aberrant textural domains appear to represent lithic clasts in the original granulitic breccia. The domain consisting of two large patches of monomineralic plagioclase represents a small fragment of coarse-grained anorthosite. Such coarse-grained areas, and areas with textures like those of the "troctolitic" domains, are common types of relict lithic clasts in granulitic breccias. The large patch bordered by a band of plagioclase certainly represents a clast, but its original texture has been obscured by the shock event.

We interpret the globules as being crystallized from melts of mafic clasts or aggregates of mafic-mineral grains. Unfortunately, none of the precursors survived the melting, so we cannot determine the original textures of these mafic materials. The globules that have straight edges or amoeboid outlines may partly preserve original clast boundaries. Those that are ovoid may have been derived from ovoid clasts, but there also may have been minor flow of the surrounding plagioclase glass during melting to accommodate rounding of

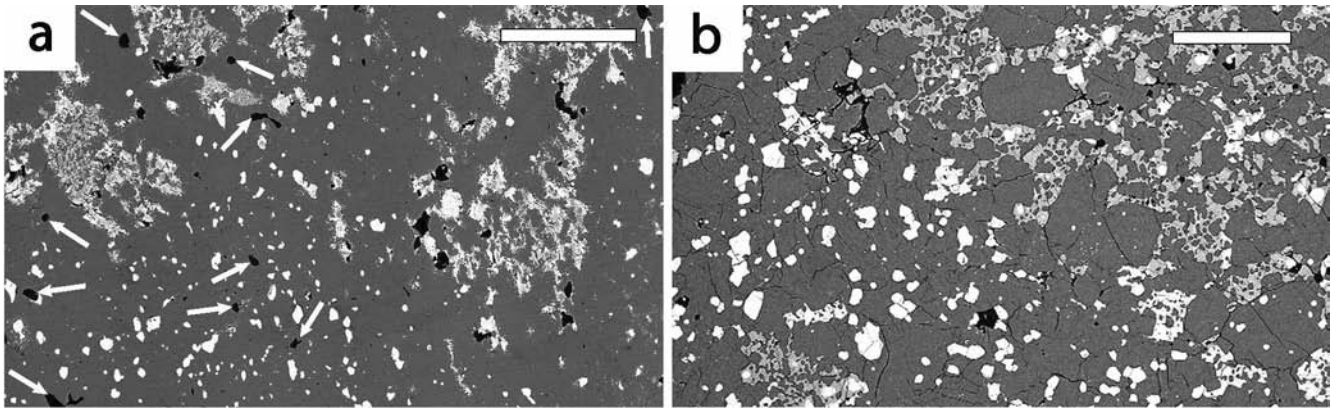

Fig. 9. BSE images of Dhofar 026 and poikilitic-granoblastic granulitic breccia 73215,339. The scale bars are 200 μm. Voids and vesicles are black; olivine is white; pyroxene is medium gray; and plagioclase is dark gray: a) Dhofar 026. Olivine-plagioclase intergrowth occupies the center, bottom center, bottom left, top center and right edge of the field. Patches of pyroxene-plagioclase intergrowth are right of center, far left of center, top left, and in the area of the scale bar. Patches of monomineralic plagioclase occur throughout the field. Small vesicles (arrows) are common in plagioclase in olivine-plagioclase intergrowth; b) sample 73215,339. This sample is a 0.53 g clast from Apollo 17 aphanitic impact melt breccia 73215; the clast was described as 73215,46,33 by James and Hammarstrom (1977) and was also studied by Cushing et al. (1999). The grain size of this poikilitic-granoblastic breccia is much coarser than that of Dhofar 026. The granoblastic intergrowth (ovoid olivine grains in plagioclase) occupies most of the lower left half of the field. The poikilitic intergrowth (plagioclase and sparse olivine grains in poikilitic pyroxene) occupies most of the upper right half of the field and a small area along the lower left edge. Subhedral plagioclase grains occur throughout both intergrowths. The granoblastic intergrowth corresponds to the olivine-plagioclase intergrowth of Dhofar 026, the poikilitic intergrowth corresponds to the pyroxene-plagioclase intergrowth, and the large plagioclase grains correspond to the monomineralic plagioclase patches.

the melt bodies. The presence of vesicles in the devitrified maskelynite grains demonstrates that the maskelynite was, indeed, plastic enough to have flowed slightly during the post-shock heating (though the flow was not extreme enough to cause extensive disruption of relict texture). Chen and El Goresy (2000) also document instances of significant flow in maskelynite. Mafic lithic clasts or rounded clots of mafic-mineral grains that could represent the precursors of the globule melts have not been described from granulitic breccias, but the range of textures of lithic clasts within granulitic breccias is not well-understood: comprehensive textural studies have been made of only one granulitic breccia (79215; Bickel et al. 1976).

Several aspects of the texture of Dhofar 026 suggest that its precursor was probably not a uniform granulitic breccia but, instead, a fragmental breccia composed almost entirely (>90%) of clasts of granulitic breccia. Passage of a shock wave through a consolidated rock produces fairly uniform shock effects. In a porous rock, however, shock-induced heating is concentrated in porous areas, and there can be localized melting in these areas (Stöffler et al. 1988). The irregular swirls and blebs of plagioclase-rich devitrified glass represent sharply defined local areas in which shock-induced heating was strongly concentrated, consistent with local, total, shock-induced melting in initially porous areas. The presence of such porous areas might simply indicate that the original granulitic breccia was locally granulated, but the observation that globules are commonly associated with the devitrified glass supports an interpretation that the precursor rock was a polymict fragmental breccia. Under this interpretation, the globules would have originally been exotic mafic clasts, surrounded by fine-grained, porous, feldspathic breccia matrix.

If, indeed, Dhofar 026 was a polymict fragmental breccia, one possible analogue from the Apollo collection is fragmental breccia 66055 (Ryder and Blair 1982). This breccia consists almost entirely of four types of fragments: granulitic breccia, plagioclase, mafic impact melt rock, and mafic glass. The 66055 granulitic breccia fragments vary somewhat in grain size and texture, but most are poikilitic-granoblastic. The glass particles include: angular fragments of clast-free glass; globules, dumbbells, and teardrops of glass containing sparse plagioclase clasts; and ovoid patches and irregular masses of clast-rich glass. A fragmental breccia similar to 66055, without the fragments of mafic impact melt rock and containing only sparse particles of mafic glass, could have been the Dhofar 026 precursor. If such a rock were the precursor, the mafic glass particles would have been the globule precursors.

Unfortunately, it is not possible to determine the type of rock that was the precursor of the Dhofar 026 granulitic breccia. The presence of lithic clasts having several different textures suggest that the precursor was polymict, but clast textures are not diverse enough for a regolith breccia or most fragmental breccias, and clasts do not appear to have been abundant. Grain size coarsens during granulitic-breccia metamorphism, especially in the finest fractions (Cushing et al. 1999); thus, the original grain size of the precursor should have been finer than the grain size of the granulitic breccia. Thus, the very fine grain size of the olivine-plagioclase intergrowth suggests that the rock may have originally been an extremely fine-grained impact-melt rock or glass containing only sparse clasts.

Summary History of Dhofar 026

Dhofar 026 was originally a granulitic breccia or a fragmental breccia consisting almost entirely of fragments of granulitic breccia. The bulk breccia was shocked to a pressure between 30 and 45 GPa, at which time it was injected with impact melt, the plagioclase was converted to maskelynite, the mafic minerals were deformed, and local patches of plagioclase-rich glass formed (probably in porous regions). After the shock, the rock experienced post-shock heating by conductive transfer of heat from the injected impact-melt veinlets (heat may also have come from an enveloping impact melt or nearby hot ejecta). The post-shock heating raised the temperature of the rock to ~1200 °C, and extensive partial melting took place. This melting was concentrated in pyroxene-rich areas, which had the lowest melting temperatures; all the pyroxene melted. Most of the pyroxene-rich melts remained near the loci where they formed, but some migrated short distances to fill fractures (these fractures might have been pre-existing or might have formed during the shock event). Small patches of ilmenite-rich melt formed in areas of pre-existing ilmenite, which had relatively low melting temperatures. Vesicles formed in the pyroxene-rich melt that later crystallized as the globules. As a result of the heating, the maskelynite devitrified and vesiculated as it crystallized, the patches of plagioclase-rich glass devitrified, and the deformed olivine recrystallized. As the rock subsequently cooled, the pyroxene-rich melts crystallized to form pyroxene-plagioclase intergrowths and globules.

We cannot determine whether or not the Dhofar 026 shock event was the impact that ejected the rock from the Moon. If the shock event was the ejection event, the rock might have cooled so quickly by radiation that partial melting could not have occurred. The cooling rate of an ejected body depends on several parameters, however, including: the mass of the body, the distribution of injected impact melt veins, and the thickness of any melt coating. Unfortunately, we do not have much data on these parameters. The meteorite appears to have been larger than the 148 g mass of the Dhofar 026 stone. Twelve other fragments found nearby (total mass: 561 g) appear to have been derived from the same meteoroid (Warren, personal communication); thus, it appears that the meteoroid broke up in the Earth's atmosphere or when it struck the ground. Dhofar 026 does not show a fusion crust; because the meteorites paired with Dhofar 026 have not yet been studied, we do not know the distribution of impact melt veins and fusion crust or whether there was a melt coating. Thus, we cannot estimate the cooling rate after ejection. There

is no evidence, however, of any shock after the partial melt crystallized. There are no shock effects, not even fracturing, that could have been produced by a subsequent event (although the breakup of the sample could have taken place along very widely spaced fractures produced by a weak shock event). Thus, all that we can conclude is that, if Dhofar 026 was ejected from the Moon by an impact event after the partial melting, that event has to have had a peak shock pressure less than a few GPa.

LUNAR GRANULITIC BRECCIA 15418

Relevance to Dhofar 026

Sample 15418 is a shocked granulitic breccia that had a history like that of Dhofar 026, but evidence for its history is better preserved than in Dhofar 026. In 15418, after the shock, conductive transfer of heat into the rock from a coating of feldspathic impact melt heated the rock; steep temperature gradients near the contact with the coating formed strong textural gradients. Because relict textures are well-preserved in the least heated parts of the rock, all the textural changes produced by the post-shock heating are easily interpreted. Comparison of the Dhofar 026 textures to similar textures in 15418 establishes the processes that operated in Dhofar 026.

Sample 15418 was previously described by Heuer et al. (1972), Christie et al. (1973), Nord et al. (1977), and Ryder (1985). The description we present herein is primarily from our own observations, supplemented by data from Nord et al. (1977) and the Lunar Sample Curatorial Facility (provided by Linda Watts). We present only the salient features; a complete description of this complex rock is beyond the scope of this study.

Sample 15418 has a gabbroic-anorthosite bulk composition (Table 6), slightly less feldspathic and slightly more ferroan than that of Dhofar 026. The similarities to Dhofar 026 are as follows: 1) 15418 was strongly shocked, and its plagioclase was converted to maskelynite; 2) after the shock, the rock was heated and partially melted; 3) the partial melt was pyroxene-rich and crystallized with igneous texture; and 4) as a result of the post-shock heating, the maskelynite devitrified and the olivine recrystallized. The major differences from Dhofar 026 are as follows: 1) the original 15418 granulitic breccia was a relatively coarse-grained granoblastic breccia; 2) near one surface, the rock shows a steep gradient in post-shock temperature and extent of melting; and 3) the rock preserves a distinct rind of impact melt rock that was probably the source of the post-shock heating.

Texture and Mineralogy

We divide 15418 into four zones: interior (no or local post-shock melting at contacts between plagioclase and pyroxene, indicating temperature near or at the solidus); intermediate (extensive post-shock melting such that all pyroxene is melted); exterior (complex swirling and mixing of mafic and plagioclase melts formed by post-shock melting); and rind (clast-poor feldspathic rocks with igneous textures, indicating temperature at or above the liquidus). We have studied the following thin sections and probe mounts: interior zone: ,98, ,155, and ,226; intermediate zone: ,18, ,19, and ,26; exterior zone: ,8, ,10, and ,26; and rind: ,8 and ,10.

The locations of the different zones within the 9 × 9 × 15 cm rock have not been mapped in detail, but processing information suggests that the bulk of the rock is made up of interior-zone material and that the intermediate zone, exterior zone, and rind are probably present only in a limited area on the N face and near the N-T edge of the rock (N, T, and S are designations assigned to rock faces during curatorial processing). Large vesicles occur only on the N face and N-T edge of the rock, suggesting that these are the only parts of the rock consisting of rind material. All of the intermediate-zone, exterior-zone, and rind materials we have examined came from a 1.5 cm-thick chip taken from the N-T edge of the rock. Interior-zone section ,98 was taken from near the center of the rock (~2–3 cm from the N-T edge chip), and interior-zone sections ,155 and ,226 were taken from the S face of the rock (~7 cm from the N-T edge chip). The entire surface of the rock appears to be a fracture surface, and there is sparse irregular fracturing throughout the rock.

Interior Zone

The interior zone shows the least modification by shock and post-shock heating. In this zone, relict texture is well-preserved; the texture is the mosaic texture typical of granoblastic granulitic breccias (Fig. 10). Triple junctions, indicating recrystallization, are well-developed (Figs. 10a and 10e). The grain size is coarser than in Dhofar 026, and there are no poikilitic or poikiloblastic areas. Most plagioclase grains are subhedral to equant anhedral and 50–500 μm across; sparse 1–5 mm grains are present. Olivine, augite, and orthopyroxene grains are equant, anhedral, and average ~50 μm across; the mafic-mineral grains occur along plagioclase grain boundaries and locally form aggregates (Fig. 10e). Sparse olivine grains as large as 2 mm are present.

All of the silicate minerals show shock effects. Augite (Fig. 10e) contains fine planar lamellae (identified as twins or pigeonite lamellae by Nord et al. [1977]), orthopyroxene shows mosaicism (Fig. 10d), olivine is locally recrystallized (Fig. 10d), and plagioclase grains (Figs. 10b and 10d) are devitrified maskelynite (aggregates of tiny elongate subgrains with similar extinction).

Locally, interior-zone samples show partial melting along mineral grain boundaries. At some contacts with plagioclase, orthopyroxene and augite grains have thin rims (Figs. 10d and 10f) of intergrown plagioclase and pyroxene that have igneous textures (plagioclase forms tiny laths

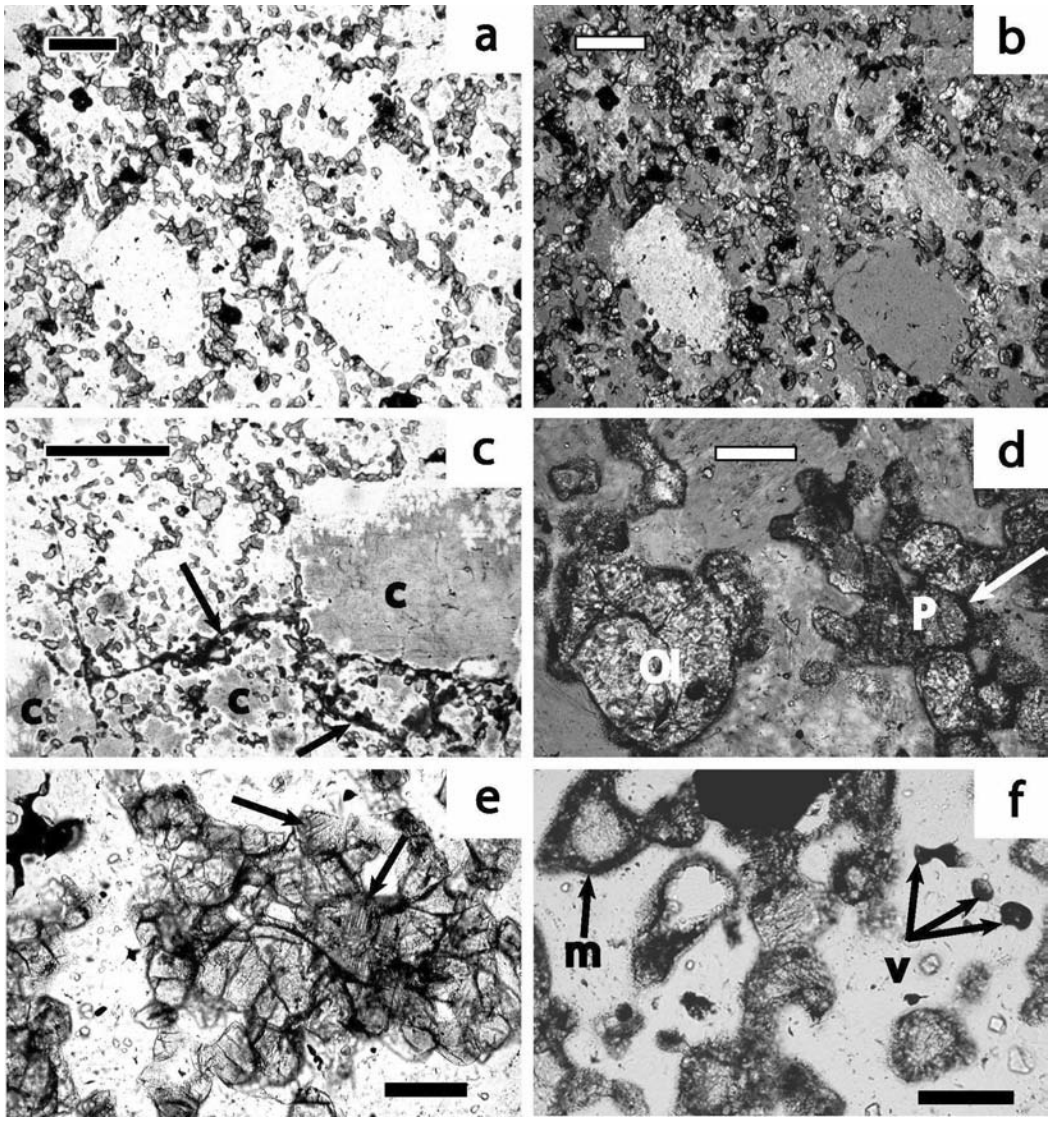

Fig. 10. Textures of 15418 interior zone samples: a) photomicrograph (plane light) of 15418,98 (section with the least post-shock heating) showing mosaic texture typical of granoblastic granulitic breccias; the scale bar is 200 μm. Small anhedral grains of mafic minerals (gray) are concentrated along boundaries of larger subhedral plagioclase grains (white); b) photomicrograph (partly crossed polarizers) of same area as (a). Each plagioclase grain is an aggregate of minute subgrains having similar extinction (texture typical of devitrified maskelynite); c) photomicrograph (plane light) of 15418,226, a section having slightly greater post-shock heating than 15418,98; the scale bar is 1 mm. The rock is cut by veinlets of brown devitrified glass (arrows). Devitrified maskelynite shows two types of devitrification texture: clear plagioclase consisting of minute subgrains having similar extinction and cloudy plagioclase (c) consisting of a coarser mosaic of grains having spherulitic extinction. Some grains of devitrified maskelynite, such as the large grain at right, contain both types of devitrification; d) photomicrograph (partly crossed polarizers) showing shock effects in 15418,226; the scale bar is 100 μm. Olivine (Ol) is a very fine recrystallized mosaic; orthopyroxene (P) shows mosaicism; plagioclase (lightest gray) is an aggregate of minute subgrains formed by devitrification of maskelynite. Some plagioclase-orthopyroxene contacts are marked by thin rims of crystallized partial melt (arrow); e) photomicrograph (plane light) of mafic-mineral aggregate in 15418,98; the scale bar is 100 μm. There is little or no post-shock grain-boundary melting. Augite shows shock-induced planar lamellae (arrows); f) photomicrograph (plane light) of 15418,226 showing considerable post-shock grain-boundary melting; the scale bar is 100 μm. Pyroxene-plagioclase contacts have rims of partial melt (m). Devitrified maskelynite contains small vesicles (v) like those in Dhofar 026 devitrified maskelynite.

enveloped by pyroxene). In areas where such melt rims are common, the devitrified maskelynite contains small vesicles (Fig. 10f) similar in size and shape to vesicles in Dhofar 026 devitrified maskelynite. Sample 15418,98 has virtually no melting at grain boundaries. Samples 15418,226 and 15418,155 show considerable variation in the degree of grain-boundary melting over distances of only a few mm, and some areas in 15418,155 show the more extensive melting that is typical of intermediate-zone samples.

In some areas, the interior-zone rock is cut by thin

veinlets of cloudy, brown, devitrified glass (Fig. 10c). The veinlets are bordered by irregular zones in which the devitrified maskelynite is cloudy (Fig. 10c). The cloudy plagioclase is a relatively coarse mosaic of equant grains with wavy, spherulitic extinction; the minute particles that cloud the plagioclase appear to be mostly of mafic minerals.

Intermediate Zone

In intermediate-zone samples, blebs of crystallized mafic melt occupy the loci of the original mafic mineral grains (Fig. 11); all pre-existing pyroxene has been melted and incorporated, along with plagioclase, into the mafic melt. Aggregates of small olivine subgrains that represent reacted, recrystallized olivine grains (Figs. 11b–11f) are found within the melt patches; the subgrains within the olivine aggregates are equant, anhedral, unshocked, and average ~5 μm across (Fig. 11b). Olivine is more magnesian near the margins of the recrystallized aggregates as a result of diffusive exchange of Fe in the olivine for Mg in the melt (Fig. 11f). Vesicles are abundant; most are 50–275 μm across and occur within the mafic melt (Figs. 11e–11f). Locally, small patches of ilmenite grains are enclosed by thin haloes of cloudy devitrified plagioclase, similar to the haloes that enclose ilmenite grains in Dhofar 026.

The crystallized mafic melt consists of very fine-grained variolitic intergrowths of pyroxene and plagioclase that grade into slightly coarser-grained subophitic intergrowths (Fig. 11b–11f). Locally in the coarser-grained intergrowths, grain boundaries are marked by slivers of opaque oxide minerals and <<1 μm blebs and septa of low-reflectivity material (probably immiscible K-Si-rich glass). Some patches of crystallized melt contain abundant skeletal opaque oxides, mostly ilmenite. As in the pyroxene-plagioclase intergrowths in Dhofar 026, some subhedral plagioclase laths at the edges of the melt patches grew as extensions of small plagioclase grains formed by devitrification of adjacent maskelynite. Throughout the intermediate zone, the melt blebs are more rounded than the original mafic mineral grains (Fig. 11a), suggesting that the surrounding plagioclase glass flowed slightly to accommodate the rounding.

In the intermediate zone, the devitrification texture of the maskelynite is variable. In some areas, the plagioclase grains are aggregates of tiny subgrains having similar extinctions (Fig. 11d). In other areas, the plagioclase consists of complexly twinned intergrowths of interpenetrating grains and aggregates of acicular plagioclase like those typical of Dhofar 026 devitrified maskelynite, only much coarser grained.

Like interior-zone sections, intermediate-zone sections show considerable textural variation. In some areas, the overall granulitic breccia texture is well-preserved, with melt blebs clearly marking the loci of original mafic mineral grains. In other areas, the melt blebs have coalesced (Fig. 11a), and the overall aggregate appears to have flowed slightly. In one probe mount, the texture grades, within one centimeter, from that typical of the intermediate zone to that typical of the exterior zone.

We have made an EMP X-ray compositional map of an area in intermediate-zone sample 15418,19 and quantitative EMP analyses of olivine and plagioclase in the same area. The X-ray map (Fig. 11f) shows that: 1) the pyroxene grains in the melt-derived intergrowth have strong normal zoning; 2) small olivine aggregates are relatively magnesian overall; and 3) large olivine aggregates are more magnesian at their edges ($Fo_{60.9–62.8}$ near the centers of two aggregates, $Fo_{66.0–71.4}$ near the edges). Nord et al. (1977) reported that interior-zone olivine is $Fo_{52–57}$, so even the least reacted olivine we analyzed is more magnesian than relict olivine. The devitrified maskelynite we analyzed ($An_{97.2–97.3}$, 0.11–0.33 wt% FeO, 0.01–0.3 wt% MgO) has essentially the same composition as the devitrified maskelynite Nord et al. (1977) analyzed in the interior zone ($An_{96–97}$, 0.10–0.30 wt% FeO, 0.03–0.07 wt% MgO). Plagioclase laths within crystallized melt blebs have essentially the same An content ($An_{97.1–97.4}$) as the devitrified maskelynite, but FeO and MgO concentrations are 0.81–0.85 and 0.65–0.68 wt%, respectively, much higher than in the devitrified maskelynite. Mixing calculations and evaluation of cation proportions by the methods of James and McGee (1992) suggest that most of the Mg and Fe are in the plagioclase structure, although we cannot rule out the possibility that some of the elevated Fe is the result of fluorescence of adjacent mafic minerals. We were unable to obtain analyses of the pyroxenes in the crystallized melt because of the small sizes of the grains.

Exterior Zone

The exterior zone was designated zone A by the Preliminary Examination Team and is referred to by this designation in lunar sample catalogs (Ryder 1985; Lunar Sample Information Catalog 1971) and by Nord et al. (1977). Exterior-zone textures are complex, and very little relict texture is preserved. Patches of crystallized plagioclase melt and crystallized, relatively mafic melts are swirled together (Figs. 12a–12c), and the melts are mixed at their contacts. Centers of the plagioclase melt patches are clear and have spherulitic devitrification textures (Figs. 12a–12c); edges of the patches are pale brown and cloudy, with devitrification textures that range from spherulitic to mosaic. Large irregular vesicles are common (Fig. 10c).

The texture and bulk composition of the relatively mafic melt is highly varied. Some mafic melt patches are well defined and have textures like those in the intermediate zone, except that grain size of the intergrowths is coarser. Contacts with adjacent plagioclase patches are interfingering: thin parallel septa of mafic minerals penetrate the crystallized plagioclase glass. In other areas, mafic melt patches contain dark-brown, equant, 40–50 μm granules that are extremely fine-grained granophyric intergrowths of plagioclase and

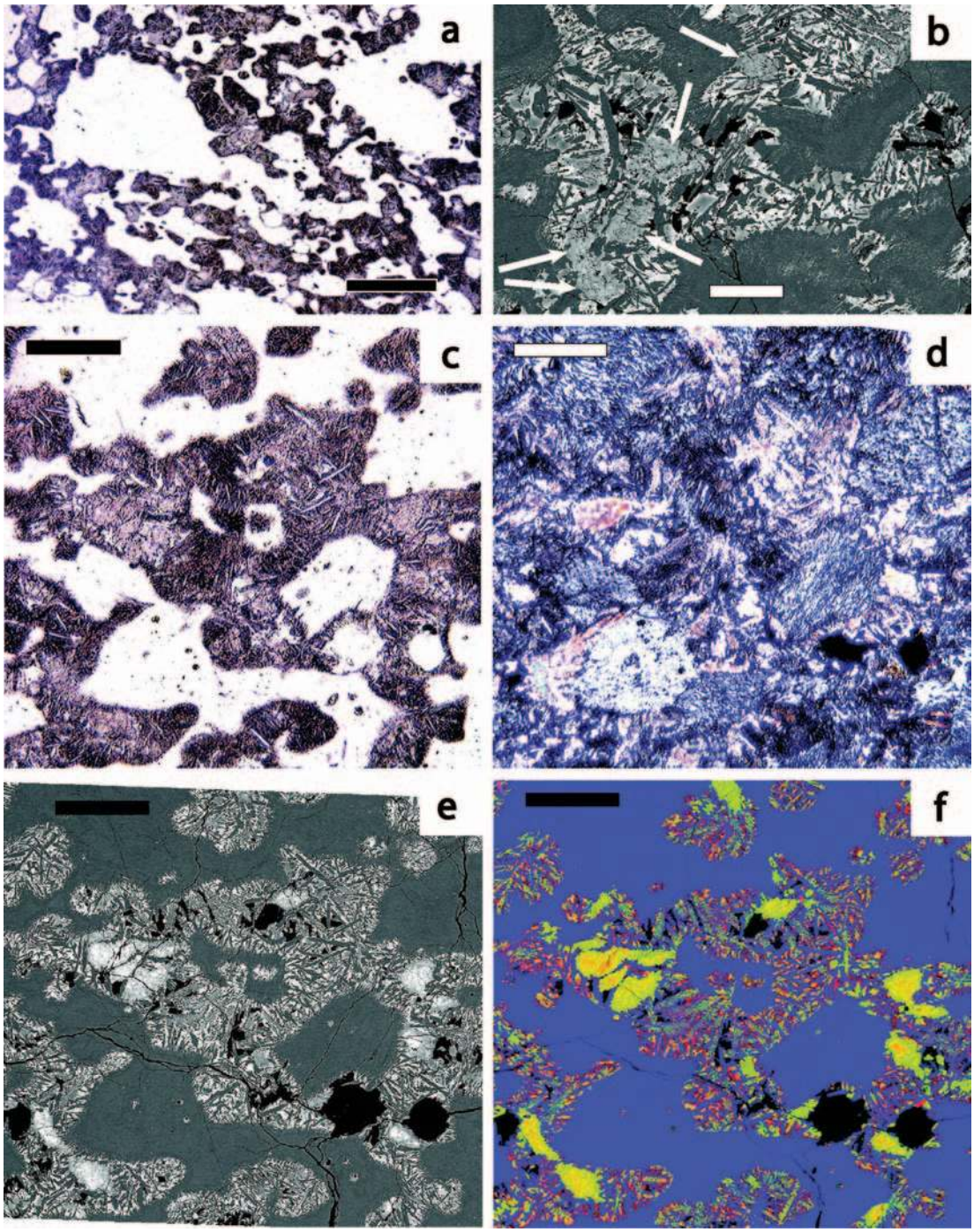

Fig. 11. Textures and compositional variations of 15418 intermediate zone samples. In BSE images, voids are black, plagioclase is dark gray, and mafic minerals are light to medium gray: a) photomicrograph (plane light) of 15418,18; the scale bar is 500 μm. All pyroxene, plus some plagioclase, is incorporated into mafic melt blebs at loci of pre-existing mafic mineral grains. The melt blebs have coalesced and show rounded outlines; b) BSE image showing variolitic to subophitic texture of melt-derived intergrowth; the scale bar is 100 μm. Arrows indicate reacted, recrystallized olivine grains; c) photomicrograph (plane light) of 15418,19; the scale bar is 200 μm. The outlines of many original plagioclase grains are preserved. The melt patches contain plagioclase needles crystallized from melt and reacted, recrystallized olivine grains (compare to [f] for location of olivines); d) photomicrograph (partly crossed polarizers) of same area as (c). Devitrified maskelynite consists of mats of tiny subparallel crystallites, and pyroxene in crystallized melt is subophitic. e) BSE image of same area as (c) and (d). Vesicles and vugs are concentrated in melt patches. Melt texture is variolitic to subophitic; f) X-ray map of same area as (c), (d), and (e). The map is a three-color image in which red = Fe, green = Mg, and blue = Ca. The colors of the phases are as follows: plagioclase, dark blue; olivine, green to yellow to orange; and pyroxenes of varied compositions, yellow to orange to red. Pyroxenes show strong normal zoning. Reacted olivine grains are relatively ferroan (orange) at their centers and relatively magnesian (green) at their edges.

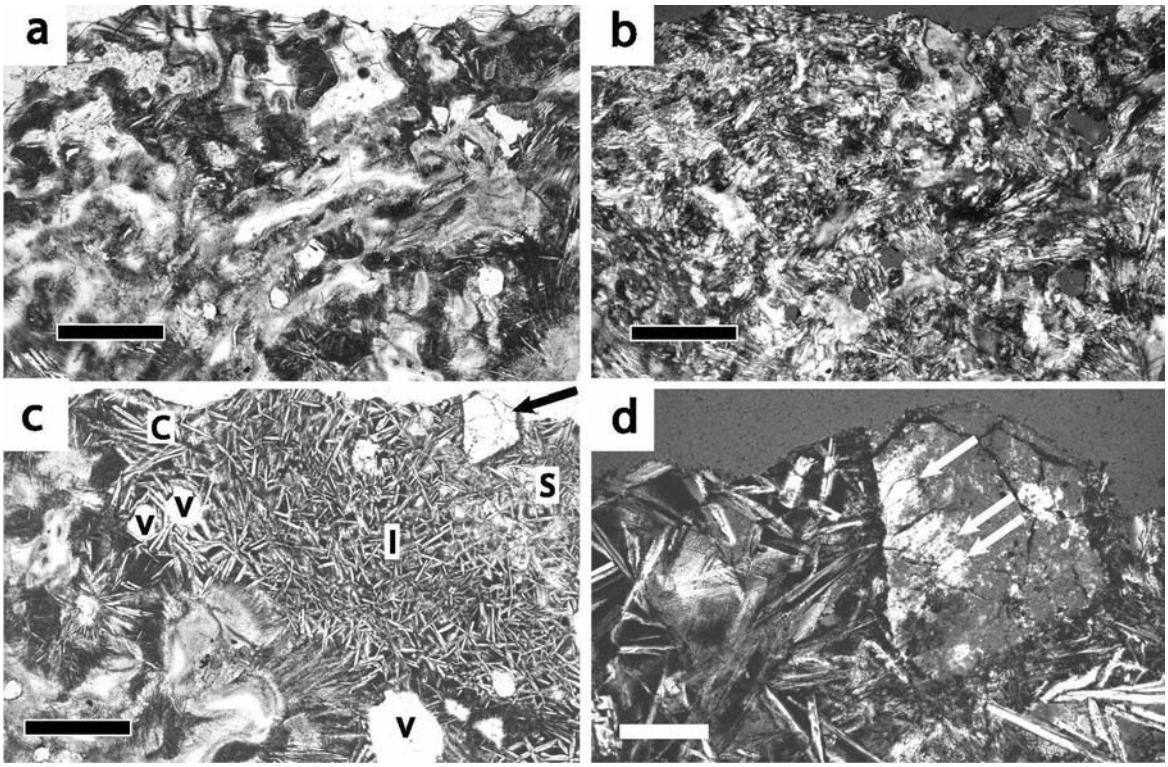

Fig. 12. Textures of 15418 exterior zone and rind samples: a) photomicrograph (plane light) of exterior zone in 15418,10; the scale bar is 500 μm. Plagioclase melt (white) and mafic mineral-rich melt (medium to dark gray) are complexly swirled together; b) photomicrograph (partly crossed polarizers) of same area as (a), showing spherulitic texture of crystallized plagioclase melt; c) photomicrograph (plane light) of exterior zone and rind in 15418,10; the scale bar is 500 μm. Exterior zone material is at the left and bottom of the field. The rind contains vesicles (v) and consists of three types of feldspathic rock with igneous textures: coarse-grained (C); "intersertal" (I); and subophitic-intergranular (S). The subophitic-intergranular rock contains an angular plagioclase clast (arrow); d) enlarged image (partly crossed polarizers) of plagioclase clast in (c); the scale bar is 100 μm. The clast is largely recrystallized (at its right and bottom); unrecrystallized areas (at left of clast) contain relict planar features (to left of and parallel to arrows).

optically continuous pyroxene. In many areas, so much plagioclase has been incorporated into the melt that its bulk composition is feldspathic. In such areas, the melts crystallized as barred pyroxene-plagioclase intergrowths in which the plagioclase forms bundles of coarse parallel or slightly radiating laths having similar extinction positions, and spaces between the laths are filled by stringers of optically continuous pyroxene.

Rind

The rind consists of three types of feldspathic rock that show igneous textures (Fig. 12c), which we designate as: 1) coarse grained; 2) "intersertal;" and 3) subophitic-intergranular. The plagioclase crystals that precipitated from the melts of the rind show no shock effects other than widely spaced fractures.

Rock of the coarse-grained zone of the rind (zone B of the Lunar Sample Information Catalog [1971]; Ryder 1985; and Nord et al. 1977) consists of randomly oriented and bundled plagioclase laths, mostly 100–200 μm long, with interstitial, fine-grained, feathery intergrowths of plagioclase, pyroxene, and mesostasis. This type of rock contains large spherical vesicles and shows sharp gradational contacts with exterior-zone melts that have a barred texture.

Rock of the "intersertal" zone of the rind is finer grained and consists of randomly oriented, euhedral plagioclase laths, mostly 40–75 μm long, with very fine-grained interstitial intergrowths similar to those in the coarse-grained zone. Rare globules of Fe-Ni metal and sparse spherical vesicles are present. This type of rock borders both exterior-zone rock and coarse-grained rind rock; the contacts are sharp gradations.

Rock of the subophitic-intergranular zone of the rind (zone C of the Lunar Sample Information Catalog [1971]; Ryder 1985; and Nord et al. 1977) consists of randomly oriented plagioclase laths that are slightly coarser (mostly 75–90 μm long) than in the "intersertal" zone, with interstices filled by subophitic to intergranular pyroxene and vugs. This type of rock borders only rock of the "intersertal" zone; the contact is a sharp gradation.

Sparse plagioclase clasts are present in the rind (we found seven in the thin sections we studied). Such clasts are found within the subophitic-intergranular and "intersertal" zones and at contacts between "intersertal" and coarse-grained zones; we found none within the coarse-grained zone.

The clasts range from 90 to 270 μm across and average 170 μm. They show varied degrees of shock and recrystallization. One clast is angular and has relict planar deformation features and extremely fine-grained recrystallization (Figs. 12c–12d); one is twinned, appears unshocked, and shows skeletal overgrowths; one is angular and shows complex twinning, shear bands, acicular subgrains, and a thin rim of very fine-grained (quenched) rind rock; and one shows sieve texture (produced by partial melting) and fine-grained recrystallization. The textures of these clasts indicate weak to moderate degrees of shock (Stöffler et al. 1991), and the rims of quenched melt on some indicate low temperatures relative to the surrounding melt.

Origin and History

The texture of the 15418 interior zone unequivocally establishes that the rock is a shocked granulitic breccia that originally had a relatively coarse granoblastic texture. Relict granulitic breccia texture is preserved to a lesser extent in the intermediate zone and is obscured in the exterior zone; the relict textures indicate that all three of these zones are parts of the same shocked granulitic breccia that experienced different degrees of post-shock heating and partial melting.

The rind was interpreted as a total melt of the 15418 granulitic breccia by Nord et al. (1977), but two aspects of the rind textures indicate that at least two zones of the rind actually represent an impact melt that enveloped the shocked granulitic breccia. First, the relatively fine grain size and "intersertal" texture of the "intersertal" zone indicate that the melt of this zone crystallized more rapidly than the melt of the subophitic-intergranular zone. The "intersertal" zone occurs between the granulitic breccia and the subophitic-intergranular zone. The presence of a zone of rapidly crystallized melt between the outermost melt of the rind and the granulitic breccia is not easily explained if the entire sample is a heated rock but can easily be explained if the rind is a separate melt that enclosed, and was quenched against, the granulitic breccia. Second, the textures of the plagioclase clasts in the "intersertal" and subophitic-intergranular melt rocks indicate that the melt that envelops them is an impact melt formed by shock-induced fusion. The plagioclase clasts show low to moderate degrees of shock; thus, they cannot be unmelted relics of the granulitic breccia because all the granulitic breccia plagioclase was strongly shocked. The observations that these clasts were not melted and that some have thin quenched rims of melt indicate that their temperatures were significantly lower than the temperature of the surrounding melt. Clasts having these characteristics are commonly entrained by impact melt during the excavation stage of crater formation (the process of incorporation of relatively unshocked clasts during flow of superheated impact melt is described by Simonds [1975] and Melosh [1989], p. 128). Melt formed by post-shock melting of the granulitic breccia should not have flowed enough to have incorporated any exotic clasts. (The origin of the coarse melt rock of the rind is not clear, but the absence of plagioclase clasts in this melt rock suggests that it may be a total melt of the granulitic breccia, as proposed by Nord et al. [1977]; alternatively, it may be a variant of the enclosing impact melt in which the plagioclase laths nucleated on the plagioclase of the granulitic breccia.) Thus, our data suggest that sample 15418 is a large clast of shocked granulitic breccia that was enveloped by feldspathic impact melt. The subophitic-intergranular texture of the outermost rind material indicates that this melt crystallized and cooled slowly, indicating a large mass of adjacent impact melt that is not now present. The impact-melt body that enveloped the granulitic-breccia clast was probably much larger than that preserved in the present volume of 15418.

Estimated Post-Shock Temperatures

We have used MELTS and experimental data to estimate the post-shock temperatures of the various zones within 15418. In the interior zone, local melting at plagioclase-pyroxene contacts suggests a post-shock temperature near the solidus of the rock; the solidus of a melt of the 15418 bulk composition (Table 6) calculated by MELTS is 1110 °C. In the intermediate zone, all the pyroxene was incorporated into the melt, but the olivine was not melted. MELTS calculations indicate a temperature for this zone between 1174 °C (the temperature at which all pyroxene would be melted) and 1222 °C (the temperature at which all olivine would be melted). A minimum temperature for the impact melt of the rind would be the liquidus temperature of the 15418 bulk composition, 1348–1341 °C (MELTS and experimental data from Uhlmann et al. [1974], respectively); this temperature is a minimum because impact melts are commonly superheated. Textures of the most extensively melted and mixed parts of the exterior zone, those in contact with the rind, indicate that these parts of the exterior zone were heated to near-liquidus temperatures.

Estimates of Shock Pressure and Predicted Post-Shock Temperature

Based on the texture of the plagioclase in the interior zone, we estimate that shock pressure in the granulitic breccia portion of sample 15418 was between 30 and 40 GPa. The plagioclase was converted to maskelynite, which requires a shock pressure between 30 GPa and 42–45 GPa, but devitrification of the maskelynite into aggregates of subgrains with similar extinction suggests a pressure no higher than 40 GPa (Ostertag and Stöffler 1982). This pressure was probably about the same throughout the granulitic-breccia portion of the sample because of its small size and low pre-shock porosity. The impact melt that forms the rind was probably shocked to a pressure ≥100 GPa. The shock effects observed in the plagioclase clasts that are included in the impact melt rind indicate varied shock pressures, from

<5 GPa (unshocked clast) to 20–30 GPa (clast with relict planar features).

As in Dhofar 026, the textures of 15418 indicate a higher post-shock temperature than predicted by the shock effects in plagioclase. In the interior zone, most of the pyroxene remained crystalline, and the textures are as expected for pyroxene shocked to 30–40 GPa; however, the devitrification of the maskelynite, the local recrystallization of the olivine, and the presence of local melting suggest that the post-shock temperature was near the solidus of the rock, more than 200 °C above the predicted temperature. The more extensive melting in the intermediate and exterior zones indicates even higher post-shock temperatures. The impact melt that enveloped the rock was apparently the source of the additional heat, as indicated by the steep gradient in the extent of partial melting of the granulitic breccia near the melt-rock rind. All the intermediate-zone and exterior-zone sections we studied were taken from an area within 1.5 cm of the rind; thus, the temperature within this region ranged from ~1174 to ~1345 °C.

The shock event that broke 15418 out of the solidified melt-rock body produced sparse irregular fracturing throughout the rock, so the peak shock pressure must have been above ~5 GPa. The plagioclase of the melt rock shows no shock-induced twinning, mosaicism, or planar features, indicating that the shock pressure was <20 GPa.

Summary History of 15418

Sample 15418 was originally a relatively coarse-grained granoblastic granulitic breccia. This granulitic breccia was shocked to a peak pressure between 30 and 40 GPa, at which time, all the plagioclase was converted to maskelynite, the pyroxenes and olivine were deformed, and the rock was enveloped by feldspathic impact melt. Conductive transfer of heat from the enveloping melt raised the post-shock temperature of the breccia, producing a steep temperature gradient near the surface of the shocked breccia clast. In the interior of the breccia, the temperature was raised to near or slightly above the solidus. The added heat caused a small amount of partial melting at plagioclase-pyroxene contacts, devitrification of the maskelynite, and local recrystallization of the olivine and pyroxenes. Small vesicles developed in the plagioclase as it devitrified.

Within a few cm of the enveloping impact melt (in the intermediate zone), the post-shock temperature of the granulitic breccia was higher and melting was more extensive. All the pyroxene, along with significant plagioclase, was incorporated into melt blebs at the loci of pre-existing mafic mineral grains. Olivine in contact with this melt became more magnesian by diffusive exchange of Fe in the olivine for Mg in the melt, and the melt vesiculated. The maskelynite devitrified, and the olivine recrystallized extensively. Some of the melt patches coalesced, and there was limited flow, but relict texture was fairly well-preserved.

Adjacent to the enveloping impact melt (in the exterior zone), temperature of the breccia was near its liquidus. Much of the breccia melted, plagioclase-rich and mafic mineral-rich melts mixed, and the entire aggregate flowed. There was local total melting. As the rock subsequently cooled, the plagioclase melts crystallized, and the mixed melts crystallized with igneous textures.

Some of the feldspathic impact melt that enveloped the granulitic breccia was quenched against the breccia and crystallized as the "intersertal" zone of the rind. The main body of the melt crystallized more slowly, forming the subophitic-intergranular zone of the rind. After crystallization, a subsequent impact broke the granulitic breccia, along with some of the enveloping impact melt, out of the crystallized melt body. Peak shock pressure during this later impact was between 5 and 20 GPa.

Implications for Dhofar 026

The textures of 15418 demonstrate the validity of the shock and post-shock history that we propose for Dhofar 026. The textures of plagioclase in Dhofar 026 are like those of devitrified maskelynite in 15418 (though finer grained), establishing that the Dhofar 026 plagioclase is indeed devitrified maskelynite. The textures of 15418 demonstrate that the processes we have inferred for Dhofar 026 are valid for a shocked rock heated, after the shock, to temperatures above its solidus by conductive heat transfer. Melting was highly localized, was concentrated at the loci of pyroxene grains, and began at contacts between plagioclase and pyroxene. The melts incorporated significant plagioclase and crystallized rapidly, with very fine-grained igneous textures and zoned pyroxenes. Considerable numbers of relict olivine grains remained after all the pyroxene had melted. Olivine in contact with the melt is more magnesian than relict olivine. Melt remained at the loci of the original mafic mineral grains unless there was significant shear.

The textures of 15418 show that proximity to impact melt can produce extensive post-shock heating and melting. Our section of Dhofar 026 does not show the strong temperature gradients we observe in 15418 sections, but the Dhofar 026 parent meteorite appears to have broken apart, and gradients may be visible if all pieces of this meteorite are examined. Our Dhofar 026 sections do not contain any of the injected melt observed by Paul Warren (personal communication), and, by analogy to 15418, we would expect temperature gradients to be strongest adjacent to the melt.

In 15418, vesicles in devitrified maskelynite are similar to those in Dhofar 026 devitrified maskelynite and are most abundant in interior-zone samples that show significant partial melting at pyroxene-plagioclase contacts. Such vesicles are not as abundant in 15418 samples that show stronger post-shock heating. These observations suggest that the vesicles formed during devitrification of the maskelynite (as observed in experiments by Ostertag and Stöffler [1982]) rather than directly as a result of the shock; thus, the presence

of vesicles in maskelynite cannot be used as an indicator of shock pressure in either rock.

Sample 15418 contains no globular bodies identical to those found in Dhofar 026, but the comparison between these two rocks does shed some light on the origin of such globules. We interpret the globules in Dhofar 026 as melted pyroxene-rich clasts; we cannot determine, however, whether these clasts were initially round or whether their outlines were modified after they melted. Textures of 15418 samples suggest that some of the rounding (though probably not all) could have occurred after the melting. In 15418 intermediate-zone sections, melt blebs have outlines that are more rounded than those of the precursor mineral grains, indicating that surrounding plagioclase glass did, indeed, flow to accommodate rounding (Fig. 11a). In fact, throughout the intermediate and exterior zones of 15418, all melt bodies have rounded outlines, suggesting pervasive small-scale flow of plagioclase glass surrounding the mafic melt blebs.

SHOCK-INDUCED HEATING VERSUS HEATING BY CONDUCTIVE HEAT TRANSFER

Dhofar 026 and 15418 provide excellent examples of the textural complexities that can result from two different, important types of heating in lunar rocks and meteorites. These two types of heating are: 1) shock-induced heating; and 2) transfer of heat by conduction into a rock from an external, higher temperature source. Distinguishing the effects of these two types of heating is critical in interpreting the histories of many lunar rocks and meteorites.

The processes of heating and melting by a shock pressure pulse are distinctive (French 1998). During passage of a shock wave, minerals are tremendously compressed, and an enormous amount of energy is deposited within them in nanoseconds to microseconds (Stöffler et al. 1991). Bonds within minerals are broken, and mineral structures can be destroyed nearly instantaneously. The response of a given mineral depends on its structure: at the same shock pressure, minerals with open structures (e.g., plagioclase) are converted to dense monomineralic liquids (Stöffler 2000; Chen and El Goresy 2002), while minerals with more dense structures (e.g., pyroxene and olivine) only show internal deformation (Stöffler et al. 1991). Deposition of energy is concentrated near voids, in porous areas (Heider and Kenkmann 2003), and along shear zones (Stöffler et al. 1991; DeCarli et al. 2002); in such areas, shock-induced temperature and pressure may be much higher than in well-indurated rock only a few μm away (DeCarli et al. 2002). A tremendous amount of energy is deposited in the rock by the shock wave, so passage of the rarefaction wave leaves the rock with a shock-induced post-shock temperature higher than its pre-shock temperature.

Because the shock wave attenuates as it moves radially outward, the peak shock pressure and shock-induced post-shock temperature decrease at increasing distances from the point of impact. In a high-energy impact, material in a hemisphere at the point of impact will have a shock-induced post-shock temperature above its vaporization temperature (Melosh 1989). Material in a hemisphere surrounding the vaporized zone will have shock-induced post-shock temperatures above its liquidus. After the shock pressure is released, the rock in this volume will melt totally, almost instantaneously; this shock-fused material is the material generally termed "impact melt." Because all the target material in which post-shock temperature is between the liquidus and the vaporization temperature is incorporated into the impact melt, much of the melt will be superheated. Material bordering the impact-melt zone will be very strongly shocked and will have shock-induced post-shock temperatures between its liquidus and solidus. Material farther out will be less strongly shocked and will have shock-induced post-shock temperatures below its solidus.

Intuitively, it seems that shock-induced partial melting would be important in high-energy impacts, but samples that show partial melting produced by high, shock-induced, post-shock temperatures are very rare (these rocks would be very strongly shocked). Theoretical calculations indicate that the volume of the target material that has post-shock temperatures between its solidus and its liquidus and, thus, could partially melt upon pressure release, is smaller than the volume that is totally fused by shock (Orphal et al. 1980). It may be that the very strongly shocked material is not preserved because of processes taking place during the excavation stage of crater formation. Because this material borders the impact melt zone and would have been granulated during the impact, much of it would probably be entrained as clasts in the superheated impact melt; the very strongly shocked, very hot clasts would then dissolve into the impact melt.

The processes and products of heating and melting by conductive heat transfer are very different than the processes and products of shock-induced heating and melting. In conductive heat transfer, the rate of heating is governed by the rate of diffusion of the heat and, thus, is much slower than in shock-induced heating. Temperature is uniform over small volumes of rock. Unlike in shock-induced melting, multiphase aggregates melt at lower temperatures than monomineralic aggregates, melting begins at grain boundaries, melting is an orderly process that can be described by phase diagrams, and mineral structure and porosity do not greatly affect melting behavior. Such conductive heating caused the post-shock devitrification of maskelynite and partial melting in both Dhofar 026 and 15418. This type of heating also causes the metamorphism of lunar granulitic breccias.

Heating by conductive heat transfer may occur in a number of situations on the Moon, the most likely of which are as follows: a rock is enveloped or injected by shock melt; a rock is buried in an ejecta deposit that contains abundant

shock melt; a rock is in the floor of an impact crater, beneath the crater's melt sheet; or a rock is near dikes, sills, or flows of mare-basalt magma. In 15418, we are fortunate that the rock retains a small part of its impact melt coating, so that the source of the post-shock conductive heating is evident. In most lunar rocks that have experienced conductive heating and melting, however, the source for the heat is not evident.

In recent descriptions of lunar meteorites, it appears that some authors have broadened the term "impact melt" to apply it to rocks affected by both shock-induced melting and melting as a result of conductive heat transfer. The term "impact melt," in most studies, has been synonymous with "shock melt" and has been applied only to rocks in which the melt fraction was produced by shock-induced fusion. In experimental and theoretical studies of impact processes (summarized by Melosh [1989]), the only material termed "impact melt" is shock-fused target material. In petrologic studies of impact products as well, only rocks in which the melt fraction formed by shock-induced fusion have been termed "impact melts" (French 1998). For example, Simonds (1975), in his classic paper on lunar impact melts, describes the melt fraction in impact melts as "superheated silicate liquid produced at the point of impact;" Simonds et al. (1976) modify this definition slightly to "superheated impact-fused material originating near the point of impact." Simonds (1975) further points out that the shock melt, during the process of excavation of the crater in which it formed, may have incorporated, by mechanical mixing, "relatively cold clasts not exposed to high shock pressures, and hence, [derived] from some distance from the point of impact." Under the terminology of Stöffler et al. (1980), shock melts that have entrained varied amounts of clasts are termed "crystalline melt breccias" or "impact melt breccias." Dence (1971) refers to such rocks found in terrestrial craters simply as impact melts. Stöffler et al. (1991; Table 1) define the terms "impact melt rocks" and "melt breccias" as rocks formed by shock-induced fusion.

Part of the rationale for applying the term "impact melt" to melts produced by melting resulting from conductive heating as well as by shock-induced fusion is the assumption that all heat for reheating of lunar rocks, after their original igneous crystallization, is ultimately derived from impacts. This assumption is not justified because it ignores the possible effects of emplacement of mare-basalt magma into and onto the lunar crust. In rocks that retain no evidence of the heat source, we cannot assume that the heat is derived from impact.

Perhaps the most important reason for not expanding the term "impact melt" to include rocks melted by conductive heat transfer, however, is the significant difference in thermal history between rocks melted by shock and by conductive heating. Even if the ultimate source of the heat in conductive heating is impact, the same rock name should not be applied to rocks that had histories that differed so greatly. We will illustrate this point by discussing the consequences of different thermal histories on ^{40}Ar-^{39}Ar age determinations. Shock melts are typically superheated; as a result, unless they are rapidly quenched, the melts are outgassed of Ar produced by prior radioactive decay of K. If a shock melt entrains cold clasts, however, the clasts may not be completely outgassed and may retain Ar; the extent of outgassing of the bulk impact melt breccia depends upon its temperature after all clasts are incorporated and its subsequent cooling rate. Thus, in ^{40}Ar-^{39}Ar studies, most impact melt breccias can be viewed as two components: a shock melt with a ^{40}Ar-^{39}Ar age that is probably that of the impact, and clasts that may retain Ar. Thus, samples of clast-poor impact melt are generally the best samples for ^{40}Ar-^{39}Ar dating of impacts (Deutsch and Schärer 1994). The very different thermal histories of rocks like Dhofar 026 and 15418, however, predict very different results for ^{40}Ar-^{39}Ar age studies. The strong shock that converted the plagioclase to maskelynite would have redistributed the Ar within the rocks but not outgassed them completely. The subsequent conductive heating that produced the partial melting might, or might not, have outgassed the rocks completely. If the rocks were completely outgassed, then ^{40}Ar-^{39}Ar studies would date the episode of conductive heating. If the rocks were not completely outgassed, then the redistribution of Ar by the shock could yield a spectrum of random "ages" that have no chronologic significance. The ^{40}Ar-^{39}Ar data for 15418 suggest that the rock was nearly completely outgassed by the conductive heating episode. The sample shows a stepwise heating plateau age of 3.98 ± 0.06 Ga (age recalculated for revised decay constants by Papike et al. [1998] from data by Stettler et al. [1973]); this plateau age probably dates the heating episode. In contrast, ^{40}Ar-^{39}Ar data for Dhofar 026 suggest that the sample was not completely outgassed at the time of the conductive heating episode. "Ages" determined by UV-laser-spot ^{40}Ar-^{39}Ar analyses range from 1.56 to 6.81 Ga (Fernandes et al. 2004); these "ages" vary widely, and some are older than the age of the Moon. The analyses appear to be measuring Ar that was grossly redistributed by the shock event; thus, the measured "ages" have no chronologic significance. Dhofar 026 was selected for a laser ^{40}Ar-^{39}Ar study on the basis of its previous classification as an impact melt because laser ^{40}Ar-^{39}Ar analyses have proved useful for resolving age differences between the shock-fused matrix and entrained clasts in impact melts (Müller et al. 1977; Eichhorn et al. 1979). Unfortunately, because Dhofar 026 had a much different thermal history than that of an impact melt, the technique was not suitable for this rock. (Cohen et al. [2002 and unpublished] also attempted ^{40}Ar-^{39}Ar age determinations on Dhofar 026 by means of stepwise heating of three microcores of olivine-plagioclase and pyroxene-plagioclase intergrowths extracted from a thick section of the meteorite. Heating of two microcores did not yield interpretable ages; the other microcore was unfortunately contaminated with flux-monitor material having an age of 569 Ma.)

As demonstrated above, shocked, partially melted rocks

such as Dhofar 026 and 15418 have thermal and mechanical histories that are grossly different from those of shock-fused impact melt rocks. Calling both types of rocks "impact melts" would be misleading. We strongly urge that the term "impact melt" continue to be restricted to rocks in which the bulk of the melt fraction has been directly generated by shock-induced fusion (and in which the melt fraction forms a volumetrically significant component of the rock).

CONCLUSION

Our studies of lunar meteorite Dhofar 026 have established that this rock is a strongly shocked granulitic breccia (or a fragmental breccia consisting almost entirely of granulitic breccia clasts) that was partially melted by post-shock heating by conductive heat transfer. The complex texture of the rock has made interpretation of its history difficult. The fact that Dhofar 026 was initially interpreted as an impact melt demonstrates that shocked lunar rocks can superficially resemble impact melts. Detailed petrographic studies of Dhofar 026, and comparison with an Apollo sample that had a similar history, were required for accurate interpretation of the origin and history of the rock. We caution that other lunar meteorites with complex textures will require similar detailed petrographic studies if their histories are to be interpreted correctly.

Many other lunar meteorites are currently being described as impact melts, and in some studies, the term appears to be used in a much broader sense than has been generally accepted in the past. The term "impact melt," in the past, has been applied only to rocks in which the melt fraction was formed by shock-induced, total fusion of the target material. The lunar-sample classification by Stöffler et al. (1980), which has been in general use for over two decades, restricts the use of the term "impact melt" to rocks in which the bulk of the melt fraction is a melt formed by shock-induced fusion. We urge that the Stöffler et al. (1980) classification be retained.

Acknowledgments–This work was supported by NASA Cosmochemistry grants NAG 5–10414 to L. A. Taylor and NAG 5–11591 to K. Keil and NASA Cosmochemistry orders W-10,088 and W-10,252 to O. B. James. We thank Allen Patchen and Kent Ross for their assistance with EMP analyses. Linda Watts researched the locations from which our thin sections and probe mounts of 15418 were taken. Discussions with Jeff Taylor, Cyrena Goodrich, Jay Melosh, and David Kring are much appreciated as are thoughtful reviews from Brad Jolliff, Allan Treiman, Ryan Zeigler, Randy Korotev, and especially Paul Warren. This research made use of NASA's Astrophysics Data System Abstract Service. This is SOEST contribution 6212 and HIGP contribution 1233.

Editorial Handling—Dr. Randy Korotev

REFERENCES

Bansal B. M., Church S. E., Gast P. W., Hubbard N. J., Rhodes J. M., and Wiesmann H. 1972. The chemical composition of soil from the Apollo 16 and Lunar 20 sites. *Earth and Planetary Science Letters* 17:29–35.

Bickel C. E., Warner J. L., and Phinney W. C. 1976. Petrology of 79215: Brecciation of a lunar cumulate. Proceedings, 7th Lunar and Planetary Science Conference. pp. 1793–1819.

Bischoff A., Weber D., Clayton R. N., Faestermann T., Franchi I. A., Herpers U., Knie K., Korschinek G., Kubik P. W., Mayeda T. K., Merchel S., Michel R., Neumann S., Palme H., Pillinger C. T., Schultz L., Sexton A. S., Spettel B., Verchovsky A. B., Weber H. W., Weckwerth G., and Wolf D. 1998. Petrology, chemistry, and isotopic compositions of the lunar highland regolith breccia Dar al Gani 262. *Meteoritics & Planetary Science* 33:1243–1257.

Blanchard D. P., Jacobs J. W., and Brannon J. C. 1977. Chemistry of ANT-suite and felsite clasts from consortium breccia 73215 and of gabbroic anorthosite 79215. Proceedings, 8th Lunar and Planetary Science Conference. pp. 2507–2524.

Chen M. and El Goresy A. 2000. The nature of maskelynite in shocked meteorites: Not diaplectic glass by a glass quenched from shock-induced dense melt at high pressures. *Earth and Planetary Science Letters* 179:489–502.

Christie J. M., Griggs D. T., Heuer A. H., Nord G. L., Jr., Radcliffe S. V., Lally J. S., and Fisher R. M. 1973. Electron petrography of Apollo 14 and 15 breccias and shock-produced analogs. Proceedings, 4th Lunar and Planetary Science Conference. pp. 365–382.

Clayton R. N. and Mayeda T. K. 1996. Oxygen isotope studies of achondrites. *Geochimica et Cosmochimica Acta* 60:1999–2017.

Cohen B. A., Taylor L. A., and Nazarov M. A. 2001. Lunar meteorite Dhofar 026: A second-generation impact melt (abstract #1404). 32nd Lunar and Planetary Science Conference. CD-ROM.

Cohen B. A., Swindle T. D., Taylor L. A., and Nazarov M. A. 2002. ^{40}Ar-^{39}Ar ages from impact melt clasts in lunar meteorites Dhofar 025 and Dhofar 026 (abstract #1252). 33rd Lunar and Planetary Science Conference. CD-ROM.

Cushing J. A., Taylor G. J., Norman M. D., and Keil K. 1999. The granulitic impactite suite: Impact melts and metamorphic breccias of the early lunar crust. *Meteoritics & Planetary Science* 34:185–195.

DeCarli P. S., Bowden E., Jones A. P., and Price G. D. 2002. Laboratory impact experiments versus natural impact events. In *Catastrophic events and mass extinctions: Impacts and beyond,* edited by Koeberl C. and MacLeod K. G. Special Paper 356. Boulder: Geological Society of America. pp. 595–605.

Dence M. R. 1971. Impact melts. *Journal of Geophysical Research* 76:5552–5565.

Deutsch A. and Schärer U. 1994. Dating terrestrial impact events. *Meteoritics* 29:301–322.

Ehmann W. D., Chyi L. L., Garg A. N., Hawke B. R., Ma M. S., Miller M. D., James W. D., Jr., and Pacer R. A. 1975. Chemical studies of the lunar regolith with emphasis on zirconium and hafnium. Proceedings, 6th Lunar and Planetary Science Conference. pp. 1351–1361.

Eichhorn G., McGee J. J., James O. B., and Schaeffer O. A. 1979. Consortium breccia 73255: Laser ^{39}Ar-^{40}Ar dating of aphanite samples. Proceedings, 10th Lunar and Planetary Science Conference. pp. 763–788.

Fagan T. J., Taylor G. J., Keil K., Bunch T. E., Wittke J. H., Korotev R. L., Jolliff B. L., Gillis J. J., Haskin L. A., Jarosewich E., Clayton R. N., Mayeda T. K., Fernandes V. A., Burgess R., Turner G., Eugster O., and Lorenzetti S. 2002. Northwest Africa

032: Product of lunar volcanism. *Meteoritics & Planetary Science* 37:371–394.

Fernandes V. A., Anand M., Burgess R., and Taylor L. A. 2004. Ar-Ar studies of Dhofar clast-rich feldspathic highland meteorites: 025, 026, 280, 303 (abstract #1514). 35th Lunar and Planetary Science Conference. CD-ROM.

French B. 1998. *Traces of catastrophe: A handbook of shock-metamorphic effects in terrestrial meteorite impact structures.* Contribution No. 954. Houston: Lunar and Planetary Institute. 120 p.

Ganapathy R., Morgan J. W., Krähenbühl U., and Anders E. 1973. Ancient meteoritic components in lunar highland rocks: Clues from trace elements in Apollo 15 and 16 samples. Proceedings, 4th Lunar and Planetary Science Conference. pp. 1239–1261.

Ghiorso M. S., and Sack R. O. 1995. Chemical mass transfer in magmatic processes IV: A revised and internally consistent thermodynamic model for the interpolation and extrapolation of liquid-solid equilibria in magmatic systems at elevated temperatures and pressures. *Contributions to Mineralogy and Petrology* 119:197–212.

Grieve R. A. F., Plant A. G., and Dence M. R. 1974. Lunar impact melts and terrestrial analogs: Their characteristics, formation, and implications for lunar crustal evolution. Proceedings, 5th Lunar and Planetary Science Conference. pp. 261–273.

Grover J. E., and Orville P. M. 1969. The partitioning of cations between coexisting single- and multi-site phases with application to the assemblages: Orthopyroxene-clinopyroxene and orthopyroxene-olivine. *Geochimica et Cosmochimica Acta* 33: 205–226.

Haskin L. A., Helmke P. A., Blanchard D. P., Jacobs J. W., and Telander K. 1973. Major and trace element abundances in samples from the lunar highlands. Proceedings, 4th Lunar and Planetary Science Conference. pp. 1275–1296.

Heider N. and Kenkmann T. 2003. Numerical simulation of temperature effects at fissures due to shock loading. *Meteoritics & Planetary Science* 38:1451–1460.

Heuer A. H., Nord G. L., Jr., Radcliffe S. V., Fisher R. M., Lally J. S., Christie J. M., and Griggs D. T. 1972. High voltage (HVEM) electron petrographic study of Apollo 15 rocks. In *The Apollo 15 lunar samples,* edited by Chamberlain J. W. and Watkins C. Houston: The Lunar Science Institute. pp. 98–102.

Higuchi H. and Morgan J. W. 1975. Ancient meteoritic component in Apollo 17 boulders. Proceedings, 6th Lunar and Planetary Science Conference. pp. 1625–1651.

Hubbard N. J., Rhodes J. M., Wiesmann H., Shih C. Y., and Bansal B. M. 1974. The chemical definition and interpretation of rock types returned from the non-mare regions of the moon. Proceedings, 5th Lunar and Planetary Science Conference. pp. 1227–1246.

James O. B. 1976. Petrology of aphanitic lithologies in consortium breccia 73215. Proceedings, 7th Lunar and Planetary Science Conference. pp. 2145–2178.

James O. B. and Flohr M. K. 1983. Subdivision of the Mg-suite noritic rocks into Mg-gabbronorites and Mg-norites. Proceedings, 13th Lunar and Planetary Science Conference. pp. A603–A614.

James O. B. and Hammarstrom J. G. 1977. Petrology of four clasts from consortium breccia 73215. Proceedings, 8th Lunar and Planetary Science Conference. pp. 2459–2494.

James O. B. and McGee J. J. 1992. Compositional variations in mare-basalt plagioclase produced by differing crystallization regimes (abstract). 23rd Lunar and Planetary Science Conference. pp. 603–604.

James O. B., Brecher A., Blanchard D. P., Jacobs J. W., Brannon J. C., Korotev R. L., Haskin L. A., Higuchi H., Morgan J. W., Anders E., Silver L. T., Marti K., Braddy D., Hutcheon I. D., Kirsten T., Kerridge J. F., Kaplan I. R., Pillinger C. T., and Gardiner L. R. 1975. Consortium studies of matrix of light gray breccia 73215. Proceedings, 6th Lunar and Planetary Science Conference. pp. 547–577.

James O. B., Lindstrom M. M., and Flohr M. K. 1989. Ferroan anorthosite from lunar breccia 64435: Implications for the origin and history of lunar ferroan anorthosites. Proceedings, 19th Lunar and Planetary Science Conference. pp. 219–243.

James O. B., Cohen B. A., and Taylor L. A. 2003. Lunar meteorite Dhofar 026: A shocked granulitic breccia, not an impact melt (abstract #1149). 34th Lunar and Planetary Science Conference. CD-ROM.

Korotev R. 1994. Compositional variation in apollo 16 impact-melt breccias and inferences for the geology and bombardment history of the central highlands of the Moon. *Geochimica et Cosmochimica Acta* 58:3931–3969.

Korotev R. L., Jolliff B. L., and Rockow K. M. 1996. Lunar meteorite Queen Alexandra Range 93069 and the iron concentration of the lunar highlands surface. *Meteoritics & Planetary Science* 31: 909–924.

Korotev R. L., Jolliff B. L., Zeigler R. A., Gillis J. J., and Haskin L. A. 2003. Feldspathic lunar meteorites and their implications for compositional remote sensing of the lunar surface and the composition of the lunar crust. *Geochimica et Cosmochimica Acta* 67:4895–4924.

Krähenbühl U., Ganapathy R., Morgan J. W., and Anders E. 1973. Volatile elements in Apollo 16 samples: Implications for highland volcanism and accretion history of the moon. Proceedings, 4th Lunar and Planetary Science Conference. pp. 1325–1348.

Lunar Sample Information Catalog, Apollo 15. 1971. MSC 03209, Lunar Receiving Laboratory, Manned Spacecraft Center, Houston.

Lunar Sample Preliminary Examination Team. 1972. Preliminary examination of lunar samples. Apollo 15 Preliminary Science Report, NASA SP-289. pp. 6-1–6-25.

Melosh H. J. 1989. *Impact cratering: A geologic orocess.* Oxford Monographs on Geology and Geophysics No. 11. New York: Oxford University Press. 245 p.

Mikouchi T., Miyamoto M., Koizumi E., Monkawa A., and McKay G. 2002. Maskelynite recrystallization: Implications for shock and reheating histories of several achondrites (abstract). *Meteoritics & Planetary Science* 37:A100.

Müller H. W., Plieninger T., James O. B., and Schaeffer O. A. 1977. Laser probe ^{39}Ar-^{40}Ar dating of materials from consortium breccia 73215. Proceedings, 8th Lunar and Planetary Science Conference. pp. 2551–2565.

Nazarov M. A., Demidova S. I., and Taylor L. A. 2003. Trace-element chemistry of lunar highland meteorites from Oman (abstract #1636). 34th Lunar and Planetary Science Conference. CD-ROM.

Nord G. L., Jr., Christie J. M., Lally J. S., and Heuer A. H. 1977. The thermal and deformational history of Apollo 15418, a partly shock-melted lunar breccia. *The Moon* 17:217–231.

Nyquist L. E., Bansal B. M., and Wiesmann H. 1975. Rb-Sr ages and initial ^{87}Sr/^{86}Sr for Apollo 17 basalts and KREEP basalt 15386. Proceedings, 6th Lunar and Planetary Science Conference. pp. 1445–1465.

Orphal D. L., Borden W. F., Larson S. A., and Schultz P. H. 1980. Impact melt generation and transport. Proceedings, 11th Lunar and Planetary Science Conference. pp. 2309–2323.

Ostertag R. and Stöffler D. 1982. Thermal annealing of experimentally shocked feldspar crystals. Proceedings, 13th Lunar and Planetary Science Conference. pp. A457–A463.

Palme H., Spettel B., Jochum K. P., Dreibus G., Weber H., Weckwerth G., Wänke H., Bischoff A., and Stöffler D. 1991. Lunar highland meteorites and the composition of the lunar crust. *Geochimica et Cosmochimica Acta* 55:3105–3122.

Papike J. J., Ryder G., and Shearer C. K. 1998. Lunar samples. In *Planetary materials,* edited by J. J. Papike. Washington D.C.: Mineralogical Society of America. pp. 5-1–5-234.

Rose H. J., Jr., Cuttitta F., Berman S., Carron M. K., Christian R. P., Dwornik E. J., Greenland L. P. and Ligon D. T., Jr. 1973. Compositional data for twenty-two Apollo 16 samples. Proceedings, 4th Lunar and Planetary Science Conference. pp. 1149–1158.

Ryder G. 1985. Catalog of Apollo 15 rocks. Curatorial Branch Publication 72, JSC 20787, NASA Johnson Space Center.

Ryder G. and Blair E. 1982. KREEP glass and the exotic provenance and formation of polymict breccia 66055. Proceedings, 13th Lunar and Planetary Science Conference. pp. A147–A158.

Sharp T. G., Xie Z., Aramovich, C., and DeCarli P. S. 2003. Pressure-temperature histories of shock-induced melt veins in chondrites (abstract #1278). 34th Lunar and Planetary Science Conference. CD-ROM.

Simonds C. H. 1975. Thermal regimes in impact melts and the petrology of the Apollo 17 station 6 boulder. Proceedings, 6th Lunar and Planetary Science Conference. pp. 641–673.

Simonds C. H., Warner J. L., Phinney W. C., and McGee P. E. 1976. Thermal model for impact breccia lithification: Manicouagan and the moon. Proceedings, 7th Lunar and Planetary Science Conference. pp. 2509–2528.

Stettler A., Eberhardt P., Geiss J., Grögler N., and Maurer P. 1973. ^{39}Ar-^{40}Ar ages and ^{37}Ar-^{38}Ar exposure ages of lunar rocks. Proceedings, 4th Lunar and Planetary Science Conference. pp. 1865–1888.

Stöffler D. 2000. Maskelynite confirmed as diaplectic glass: Indication for peak shock pressures below 45 GPa in all martian meteorites (abstract # 1170). 31st Lunar and Planetary Science Conference. CD-ROM.

Stöffler D., Knöll H. D., Marvin U. B., Simonds C. H., and Warren P. H. 1980. Recommended classification and nomenclature of lunar highland rocks—A committee report. In *Proceedings of the Conference on Lunar Highlands Crust,* edited by Papike J. J. and Merrill R. B. *Geochimica et Cosmochimica Acta* 12:51–70.

Stöffler D., Bischoff A., Buchwald V., and Rubin A. E. 1988. Shock effects in meteorites. In *Meteorites and the early solar system,* edited by Kerridge J. F. and Matthews M. S. Tucson: University of Arizona Press. pp. 165–202.

Stöffler D., Keil, K., and Scott E. R. D. 1991. Shock metamorphism of ordinary chondrites. *Geochimica et Cosmochimica Acta* 55: 3845–3867.

Taylor L. A., Nazarov M. A., Cohen B. A., Warren P. H., Barsukova L. D., Clayton R. N., and Mayeda T. K. 2001. Bulk chemistry and oxygen isotopic compositions of lunar meteorites Dhofar 025 and Dhofar 026 (abstract #1985). 32nd Lunar and Planetary Science Conference. CD-ROM.

Taylor S. R. 1982. *Planetary science: A lunar perspective.* Houston: Lunar and Planetary Institute. 481 p.

Taylor S. R., Gorton M. P., Muir P., Nance W., Rudowski R., and Ware N. 1973. Lunar highlands composition: Apennine front. Proceedings, 4th Lunar and Planetary Science Conference. pp. 1445–1459.

Uhlmann D. R., Klein L., Kritchevsky G., and Hopper R. W. 1974. The formation of lunar glasses. Proceedings, 5th Lunar Science Conference. pp. 2317–2331.

Walker D., Longhi J., Grove T. L., Stolper E., and Hays J. F. 1973. Experimental petrology and origin of rocks from the Descartes highlands. Proceedings, 4th Lunar and Planetary Science Conference. pp. 1013–1032.

Wänke H., Palme H., Kruse H., Baddenhausen H., Cendales M., Dreibus G., Hofmeister H., Jagoutz E., Palme C., Spettel B., and Thacker R. 1976. Chemistry of lunar highland rocks: A refined evaluation of the composition of the primary matter. Proceedings, 7th Lunar and Planetary Science Conference. pp. 3479–3499.

Warren P. H. 1997. The unequal host-phase density effect in electron probe defocused beam analysis: An easily correctable problem (abstract). 28th Lunar and Planetary Science Conference. pp. 1497–1498.

Warren P. H., Taylor L. A., Kallemeyn G., Cohen B. A., and Nazarov M. A. 2001. Bulk-compositional study of three Dhofar lunar meteorites: Enigmatic siderophile element results for Dhofar 026 (abstract #2197). 32nd Lunar and Planetary Science Conference. CD-ROM.

Zipfel J., Spettel B., Palme H., Wolf D., Franchi I., Sexton A. S., Pillinger C. T., and Bischoff A. 1998. Dar al Gani 400: Chemistry and petrology of the largest lunar meteorite (abstract). *Meteoritics & Planetary Science* 33:A171.